

AD-A134 715

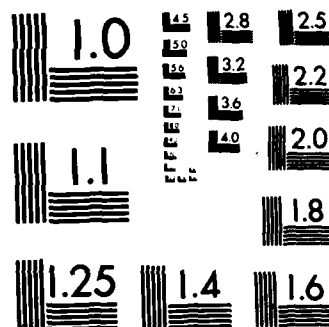
METHODOLOGY FOR THE CALCULATION OF A SHALLOW-WATER WAVE 1/1  
CLIMATE(U) ARMY ENGINEER WATERWAYS EXPERIMENT STATION  
VICKSBURG MS R E JENSEN SEP 83 WIS-8

UNCLASSIFIED

F/G 8/3

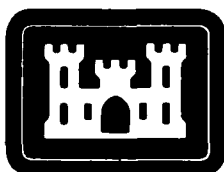
NL



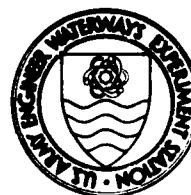


MICROCOPY RESOLUTION TEST CHART  
NATIONAL BUREAU OF STANDARDS-1963-A

A134715



12



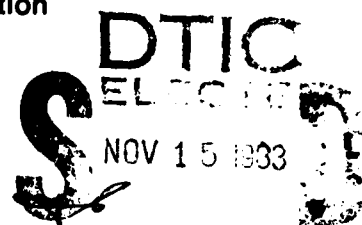
# METHODOLOGY FOR THE CALCULATION OF A SHALLOW-WATER WAVE CLIMATE

by

Robert E. Jensen

Coastal Engineering Research Center  
U. S. Army Engineer Waterways Experiment Station  
P. O. Box 631, Vicksburg, Miss. 39180

WIS Report 8  
September 1983



Approved For Public Release; Distribution Unlimited

## WAVE INFORMATION STUDIES OF U.S. COASTLINES

Prepared for Office, Chief of Engineers, U.S. Army  
Washington, D.C. 20314

DTIC FILE COPY

83 11 13 005

Destroy this report when no longer needed. Do not return  
it to the originator.

The findings in this report are not to be construed as an official  
Department of the Army position unless so designated  
by other authorized documents.

This program is furnished by the Government and is accepted and used  
by the recipient with the express understanding that the United States  
Government makes no warranties, expressed or implied, concerning the  
accuracy, completeness, reliability, usability, or suitability for any  
particular purpose of the information and data contained in this pro-  
gram or furnished in connection therewith, and the United States shall  
be under no liability whatsoever to any person by reason of any use  
made thereof. The program belongs to the Government. Therefore, the  
recipient further agrees not to assert any proprietary rights therein or to  
represent this program to anyone as other than a Government program.

The contents of this report are not to be used for  
advertising, publication, or promotional purposes.  
Citation of trade names does not constitute an  
official endorsement or approval of the use of  
such commercial products.

Cover photo by Steve Lissau. Photo originally ap-  
peared in *Oceans*, a publication of the Oceanic  
Society, Vol. 12, No. 1, Jan-Feb 1979.

Unclassified

SECURITY CLASSIFICATION OF THIS PAGE (When Data Entered)

REPORT DOCUMENTATION PAGE		READ INSTRUCTIONS BEFORE COMPLETING FORM
1. REPORT NUMBER WIS Report 8	2. GOVT ACCESSION NO. <b>A134715</b>	3. RECIPIENT'S CATALOG NUMBER
4. TITLE (and Subtitle)  METHODOLOGY FOR THE CALCULATION OF A SHALLOW-WATER WAVE CLIMATE	5. TYPE OF REPORT & PERIOD COVERED  Final report	
	6. PERFORMING ORG. REPORT NUMBER	
7. AUTHOR(s)  Robert E. Jensen	8. CONTRACT OR GRANT NUMBER(s)	
9. PERFORMING ORGANIZATION NAME AND ADDRESS U. S. Army Engineer Waterways Experiment Station Coastal Engineering Research Center, P. O. Box 631, Vicksburg, Miss. 39180	10. PROGRAM ELEMENT, PROJECT, TASK AREA & WORK UNIT NUMBERS	
11. CONTROLLING OFFICE NAME AND ADDRESS Office, Chief of Engineers U. S. Army Washington, D. C. 20314	12. REPORT DATE September 1983	
	13. NUMBER OF PAGES 80	
14. MONITORING AGENCY NAME & ADDRESS (if different from Controlling Office)	15. SECURITY CLASS. (of this report)  Unclassified	
	15a. DECLASSIFICATION/DOWNGRADING SCHEDULE	
16. DISTRIBUTION STATEMENT (of this Report)  Approved for public release; distribution unlimited.		
17. DISTRIBUTION STATEMENT (of the abstract entered in Block 20, if different from Report)		
18. SUPPLEMENTARY NOTES  Available from National Technical Information Service, 5285 Port Royal Road, Springfield, Va. 22161		
19. KEY WORDS (Continue on reverse side if necessary and identify by block number)  Atlantic coast Shallow water waves Wave hindcast Wave transformation		
20. ABSTRACT (Continue on reverse side if necessary and identify by block number)  This report describes the methodology employed to generate 20 years of wave conditions in 10-m water depths as part of the Wave Information Study. Descriptive techniques (time series plots, cross plots, and percent occurrence plots) are employed to compare recorded and computed wave heights and periods at six locations along the Atlantic coast.		

DD FORM 1 JAN 73 1473

EDITION OF 1 NOV 65 IS OBSOLETE

Unclassified

SECURITY CLASSIFICATION OF THIS PAGE (When Data Entered)

## Preface

In late 1976, a study to produce a wave climate for U. S. coastal waters was initiated at the U. S. Army Engineer Waterways Experiment Station (WES). The Wave Information Study (WIS) was authorized by the Office, Chief of Engineers, U. S. Army, as a part of the Coastal Field Data Collection Program which is managed by the U. S. Army Coastal Engineering Research Center. The U. S. Army Engineer Division, South Atlantic, and the U. S. Army Engineer Division, New England, also authorized funds during the initial year of this study (FY 1978) to expedite execution of the Atlantic coast portion of this program.

This report, the eighth in a series, presents the theoretical development of the Phase III portion of WIS which is employed to calculate wave information in shallow water. The study was conducted in the Hydraulics Laboratory under the direction of Mr. H. B. Simmons, Chief of the Hydraulics Laboratory, Dr. R. W. Whalin, former Chief of the Wave Dynamics Division, and Mr. C. E. Chatham, Jr., Acting Chief of the Wave Dynamics Division. Mr. J. H. Lockhart, Jr., is the Office, Chief of Engineers, Technical Monitor for the Coastal Field Data Collection Program. This report was prepared by Dr. R. E. Jensen with assistance from Mr. W. D. Corson and Ms. J. H. Messing. Initial work in the theoretical treatment of the Phase III methodology was performed with the help of Dr. D. T. Resio.

Commanders and Directors of WES during the conduct of the study and the preparation and publication of this report were COL John L. Cannon, CE, COL Nelson P. Conover, CE, and COL Tilford C. Creel, CE. Technical Director was Mr. F. R. Brown.



Classification for	
THIS GRADE	<input checked="checked" type="checkbox"/>
THIS TAB	<input type="checkbox"/>
Unannounced	<input type="checkbox"/>
Justification	
By _____	
Date _____	
Classified by _____	
Declassify on _____	
A-1	

## Contents

	<u>Page</u>
Preface . . . . .	1
Introduction . . . . .	3
Development of Phase III Methodology . . . . .	5
Brief perspective of previous methodologies . . . . .	5
An alternate approach . . . . .	7
Representation of Offshore Wave Conditions for Wave Transformation . . . . .	8
Processes Involved in Nearshore Wave Transformations . . . . .	13
Conservative processes . . . . .	14
Nonconservative processes . . . . .	16
Comparisons . . . . .	24
WIS Phase III hindcast wave data . . . . .	26
Measured wave data . . . . .	26
Time-history comparisons . . . . .	29
Percent occurrence comparisons . . . . .	31
Extreme storm event comparisons . . . . .	37
Summary and Conclusions . . . . .	42
References . . . . .	47
Tables 1 and 2	
Plates 1-6	
APPENDIX A: Mathematical Treatment of the Transformation of Probabilities from One Coordinate System into Another . . .	A1
APPENDIX B: Comparison of Spectral and Monochromatic Representation for Refraction and Shoaling . . . . .	B1
APPENDIX C: Plots of $H_s$ and $T_p$ Versus Time . . . . .	C1
APPENDIX D: Notation . . . . .	D1

METHODOLOGY FOR THE CALCULATION OF A  
SHALLOW-WATER WAVE CLIMATE

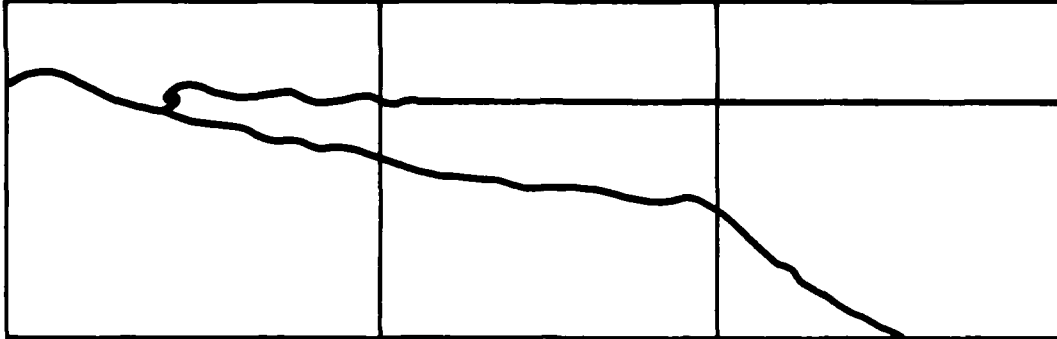
Introduction

1. The primary purpose of the Wave Information Study (WIS) is to produce useful, reliable wave data for planning and design in coastal waters. During the last 6 years, a methodology has evolved to simulate the offshore wave climate via numerical procedures. Extensive efforts have been directed into problems of wind and wave prediction over large ocean areas from historical records. Reports 1-7 in this series document various portions of this work. From comparisons of hindcast and measured data sets, it would appear that the climatological characteristics of the simulated data in the offshore area are quite similar to those of the measured data (Corson and Resio 1981). The task of accurately transforming these offshore data into the nearshore region now assumes a critical role in the final stage of obtaining the overall WIS goal.

2. Previous approaches to nearshore wave transformations have concentrated on the calculation of a limited number of wave conditions over very small spatial areas. The reason for this is that, typically, the results are needed at a particular site for some specific design or planning consideration. While this approach is convenient when transforming a small number of given offshore wave conditions into nearshore wave conditions, it becomes very cumbersome when attempting to define a nearshore wave climate over 20 years time along thousands of miles of coast. Instead, the WIS approach has been to analyze successive nested scales of natural organization in time and space along a coast. As shown in Figure 1, this leads to a three-phase organization of WIS, with various processes becoming dominant at different distances from a coast.

3. It is impossible to foresee every site at which detailed wave information will be required for specific projects in the future. Also, it is not cost-effective to perform detailed calculations on an ultra-fine grid for all coastal areas, since most of this information would





ATMOSPHERIC RESPONSE SCALES	NEARSHORE ZONE		
	SHELF ZONE		
	DEEP OCEAN		
	SYNOPTIC, MESOSCALE CONVECTIVE	MESOSCALE AND SYNOPTIC	SYNOPTIC AND LARGE SCALE
	$\Delta x$ LESS THAN 10 MILES $\Delta t$ LESS THAN 3 HOURS	$\Delta x$ 10'S OF MILES $\Delta t$ 3 TO 6 HOURS	$\Delta x$ 100'S OF MILES $\Delta t$ GREATER THAN 6 HOURS
WAVE PROCESSES	AIR-SEA INTERACTION REFRACTION DIFFRACTION SHOALING BOTTOM FRICTION LONG WAVES (TIDES AND SURGE)	AIR-SEA INTERACTION REFRACTION DIFFRACTION SHOALING BOTTOM FRICTION	AIR-SEA INTERACTION
	WAVE TRANSFORMATION	SECONDARY ENERGY SOURCE WAVE TRANSFORMATIONS	PRIMARY ENERGY SOURCE

Figure 1. Schematic representation of the three phases of the WIS

never be needed. Consequently, the Phase III data must be computed in such a manner as to be representative of some length of coast which is sufficient to be useful for most projects, while sufficiently large to filter out many spurious local effects. As shown in Plates 1-6, 10-mile coastal segments were selected to meet this requirement. Small-scale variations in wave climate within a 10-mile segment can be treated as perturbations on this Phase III scale if additional spatial detail is required.

4. Several advantages are associated with the selection of this 10-mile scale in Phase III. The most notable of these is probably the dramatic decrease in cost of computation. This is particularly important

since the processes involved in nearshore wave transformation are not completely understood at the present time (Vincent 1982). It is expected that results in the nearshore zone may have to be recomputed at some later time as an understanding of, and ability to model, wave transformation processes increases. Thus it would not seem reasonable to develop extremely costly, time-consuming methods for the present Phase III calculations.

5. Although the techniques used must be general in terms of distance along the coast, recent field evidence has suggested that significant variations in wave energy occur systematically in the onshore-offshore direction. These effects will not average out over longshore distance; consequently, all Phase III results must be referenced to a particular depth. In very shallow water, the effects of depth become so dominant that variations in mean water levels (tides, surges, setup, etc.) are the controlling factors in the external portion of the wave-height distribution. Three situations in wave climate estimations can be related to the relative importance of water-level variations. In the innermost and outermost regions, water-level variations and wave-height variations can be treated independently. However, in the intermediate region, which typically is the area of primary interest, the behavior of both must be considered together in the formulation of a wave climate. For this first Phase III report, a 10-m depth has been chosen as representative of nearshore conditions while not being too dependent on most water-level variations.

6. It should also be noted that the present report, like the previous Phase I and Phase II reports, is limited to extratropical conditions. That portion of the wave climate contributed by tropical storms will be added to this data set in a later report.

#### Development of Phase III Methodology

##### Brief perspective of previous methodologies

7. Many different techniques are presently used to transform

deepwater wave information into shallow water. In general, these techniques can be separated into two broad classes, those which transform individual wave conditions and those which transform probability distributions of wave parameters from one space (or water depth) to another.

8. The first class of techniques generally transforms a specified wave condition at a boundary (defined by a set of wave parameters), through some intermediate water depth region, into shallow water. Typically, this method is based on linearized formulations of monochromatic wave theories where the dependent wave parameters are influenced by shallow-water effects (wave shoaling, refraction, diffraction, bottom friction, breaking, etc.) (Skovgaard, Jonssen, and Bertelsen 1975). More recently, computer codes based on approximations to dispersive long waves have been used to calculate shallow-water wave transformations which include additional nonlinear effects. However, these codes tend to be quite expensive to run; and in most open-coast areas, the results obtained are quite similar to linear theory. A third approach, used in some studies, involves the transformation of wave spectra propagating into shallow water. This method usually requires extensive amounts of computer time since each frequency-direction component of the spectrum must be propagated and have its energy source/sink integration performed individually (Hsiao 1978).

9. In the second class of techniques, a Jacobian matrix operator is used to transform distribution of wave heights, periods, and directions in deep water into corresponding shallow-water distributions as shown in Appendix A.

10. A major problem in this approach lies in the evaluation of the Jacobian. If an analytical method is applied for this purpose, only certain classes of functions can be admitted into the interrelationships between different wave parameters. This restriction could be overcome through a purely numerical approach; however, the method would still lose all information on specific events (i.e. individual storms) and would not provide a very accurate description of the external portion of the nearshore wave population.

### An alternate approach

11. Since neither of the traditional approaches to the estimation of nearshore wave characteristics seemed appropriate, a third approach to the problem of nearshore wave transformations was developed specifically to meet the needs of the Phase III portion of WIS. It should be recognized at the outset of this discussion that the primary objective of this new approach is to maximize calculation efficiency rather than to introduce a new wave transformation technique. This increase in efficiency is accomplished by recognizing that over sufficiently small intervals, wave parameters may be considered approximately equal. In other words, a 1.01-m wave height is not essentially different from a 1.00-m height in most applications, an 8.42-sec wave period is approximately equivalent to an 8.4-sec wave period, and so on.

12. The first problem which must be resolved in this approach is how many wave parameters are required to represent deepwater wave conditions such that all basic information affecting the nearshore transformation process is retained. If this number is sufficiently small, and if the number of increments needed to cover the range of parameter values expected is reasonable, then a discretized approach is quite advantageous to performing individual calculations. For example, if the computations were made on an individual basis at each Phase III site, almost 10 million transformations would be required to span the 20-year period of the hindcast at 3-hr intervals. However, if only three parameters, each spanned by 20 intervals, were required to obtain adequate resolution, then only  $(20)^3$  or 8,000 transformation calculations would be required. More generally, an n-parameter transformation would require  $N^*$  calculations,

$$N = \prod_{i=1}^n m_i \quad (1)$$

where  $m_i$  is the number of intervals used to resolve the  $i^{\text{th}}$

---

\* For convenience, symbols are listed and defined in the Notation (Appendix D).

parameter. Since these transformations have been generalized for parallel bottom contours, these calculations would suffice for all 166 shoreline segments for a given depth.

13. It is important to note here that other than the parallel bottom assumption, no assumptions have been made regarding the nature of the transformation process. Consequently, any number of transformation mechanisms can be considered within the framework of this approach. This means that it is easy to add to or delete mechanisms from the computer analog. This algorithm is used to establish a matrix of  $N$  transformed values for each of the  $i^{\text{th}}$  parameters. When the individual transformations are performed, the incremental deepwater parameter values can then be viewed as indices to a matrix of transformed values; thus we have for any individual  $n$ -parameter transformation as a matrix formulation given by

$$\begin{aligned} P'_1 &= T_1(I_1, I_2, \dots, I_n) \\ P'_2 &= T_2(I_1, I_2, \dots, I_n) \\ P'_n &= T_n(I_1, I_2, \dots, I_n) \end{aligned} \quad (2)$$

where  $P'_i$  are the nearshore wave parameter values,  $T_i$  are the transformation matrices, and  $I_n$  are the incremental values of the deepwater parameters. The only calculations required are the conversions of the continuous values of the deepwater parameters  $P_i$  into the referencing indices  $I_n$ , which usually require only a single multiplication.

#### Representation of Offshore Wave Conditions for Wave Transformation

14. In the Phase II wave model, 20 discretized frequency increments and 16 discretized angle increments were used to approximate continuous two-dimensional wave spectra (Resio 1981). If all 320 elements in the 16-x-20 array were treated as independent, the value of  $N$  would become ridiculously large in an analysis of the type just described. On the other hand, if the spectra were reduced to simple monochromatic wave

trains, significant information important to nearshore wave transformations would be lost. An approach that attempts to retain the organized structure of the spectra and to include these effects into nearshore wave transformations would be to use a parametric representation of the offshore wave climate. The solutions, although they can be computed as two-dimensional spectra, are effectively limited to the parameter space itself. Hasselmann et al. (1973 and 1976) give good descriptions of the use of parametric models for wave generation and propagation. The principle in this case is quite similar.

15. Most parameterizations of wave spectra to date have treated the frequency variation and angular variation of energy density separately. Thus the two-dimensional spectrum can be written as

$$E_2(f, \theta) = E_1(f) \phi(\theta)$$

or

$$E_2(f, \theta) = E_1(f) \phi(\theta, f)$$

where  $E_2$  is the two-dimensional spectrum (in frequency  $f$  and direction  $\theta$ ),  $\phi$  is a normalized angular distribution function and  $E_1$  is the one-dimensional spectrum defined as

$$E_1(f) = \int_0^{2\pi} E_2(f, \theta) d\theta$$

The number of parameters used to represent a spectrum varies as a function of the detail one wishes to retain. The classic Pierson-Moskowitz spectrum (Pierson and Moskowitz 1964) can be written in the form

$$E_1(f) = \frac{0.0081g^2 f^{-5}}{(2\pi)^4} \exp \left[ -1.25 \left( \frac{f}{f_m} \right)^{-4} \right] \quad (3)$$

where  $g$  is acceleration due to gravity,  $f$  is frequency, and  $f_m$  is the frequency of the spectral peak. Essentially, there is only one free

parameter,  $f_m$ , in this representation. More recently, the JONSWAP spectrum containing three free parameters was introduced by Hasselmann et al. (1973)

$$E_1(f) = \frac{\alpha g^2 f^{-5}}{(2\pi)^4} \exp \left[ -1.25 \left( \frac{f}{f_m} \right)^{-4} \right] \delta^\nu \quad (4)$$

where  $\alpha$ ,  $f_m$ , and  $\delta$  are all free parameters and  $\nu$  is a given function of  $(f/f_m)$ . The JONSWAP spectrum is somewhat cumbersome to treat analytically and for all but the last stage of wave growth  $\nu$  is taken to be a constant equal to 3.3. In many recent field experiments of active wave growth, the JONSWAP spectrum has been shown to provide a reasonably good approximation to the measured spectrum; however, an almost equivalent but much simpler form for these spectra was postulated by Kitaigorodskii (1962) on the basis of similarity theory

$$\begin{aligned} E_1(f) &= \frac{\alpha g^2 f^{-5}}{(2\pi)^4} \quad \text{for } f \geq f_m \\ &= \frac{\alpha g^2 f_m^{-5}}{(2\pi)^4} \exp \left[ 1 - \left( \frac{f}{f_m} \right)^{-4} \right] \quad \text{for } f < f_m \end{aligned} \quad (5)$$

This form has only two free parameters  $\alpha$  and  $f_m$ ; consequently, a simple relationship between total wave energy and these parameters exists, i.e.

$$E_o = \int_0^\infty E_1(f) df = \lambda \alpha g^2 f_m^{-4} \quad (6)$$

where  $\lambda$  is a constant.

16. Equation 5 should provide a good description of the one-dimensional spectrum under active wave generation conditions; therefore it provides a description of what is typically referred to as the local sea. The spectral shape could be made increasingly complex by introducing additional spectral parameters. Since the portion of the spectrum occupied by the local sea has been defined, the major contributions remaining in the spectrum must come from swell advected into coastal areas.

Since the parameters  $\alpha$  and  $f_m$  are contained within all Phase II wave records, the distinction between sea and swell here is not at all arbitrary.

17. This separation of the wave records into sea and swell permits distinctly different approaches to the treatment of the frequency and directional characteristics of these wave trains. Swell that has propagated beyond its area of generation usually contains almost all of its energy in a narrow frequency and direction band. Thus swell can be adequately described as a unidirectional, monochromatic wave train impinging on a coast. On the other hand, the local sea tends to be quite broad-banded in direction as well as frequency. Therefore a directional distribution function must be included for the local sea in order to account for this. Resio (1978) has shown that longshore energy fluxes (and associated longshore sediment transport rates) can be very significantly affected by this directional distribution of energy in a spectrum; thus it is important to include such effects in the nearshore transformation. A reasonable approximation to average directional distributions for observed spectra is given by a  $\cos^4 \theta$  distribution of energy for deepwater input conditions to the Phase III parametric spectral form

$$E_2(f, \theta) = E_1(f) \frac{8}{3\pi} \cos^4 (\theta - \bar{\theta}) \quad (7)$$

where  $E_1(f)$  is given by Equation 5 and  $\bar{\theta}$  is the central angle of the spectrum.

18. As additional information accumulates relative to a better definition of directional spectral characteristics (Vincent 1982), improved directional distribution functions can be inserted into input conditions to the Phase III data if desired.

19. At this point, each of the two kinds of wave trains seen along a coast have been shown to be representable by three parameters: wave height (H), wave period (T), and wave direction ( $\theta$ ) for the unidirectional monochromatic swell and  $\alpha$ ,  $f_m$ , and  $\bar{\theta}$  for the local sea. For consistency, if we define a period of the spectral peak as  $T_p = f_m^{-1}$



and use Equation 6 to obtain wave height as a function of  $\alpha$  and  $T_p$ , then both wave trains can be described by comparable parameters  $H$ ,  $T$ , and  $\theta$ . It should be recognized that this by no means restricts the local sea to unidirectional monochromatic waves, but rather only to a fixed deepwater, spectral shape.

20. Due to the nature of the definition of local sea, only one such wave train can exist in one place at one time; however, this is not the case for swell, since it can propagate from various source regions into a particular coastal area. An analysis of wave generation areas in the Atlantic Ocean indicates that one swell wave train should suffice to provide an adequate description of the significant aspects of nearshore wave climate generated by storms which have: (a) passed a site and are moving away or (b) passed along the coast some distance offshore (Figure 2).

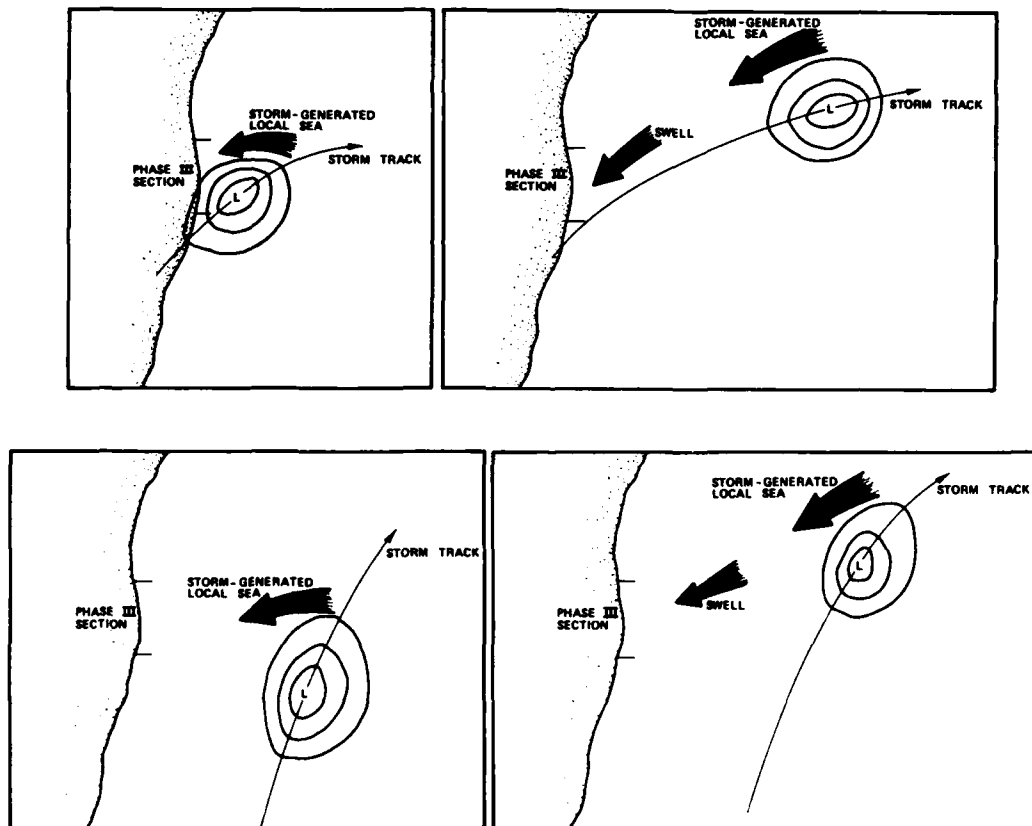


Figure 2. Generalized storm tracks along the Atlantic coast

21. Figure 3 summarizes the previous discussion regarding the representation of wave propagation into the coast. As seen here, two independent wave trains are considered superimposed at the coast: a local sea described by three free parameters defining a two-dimensional spectrum, and a swell wave train from passing storms described by three free parameters defining unidirectional, monochromatic waves.

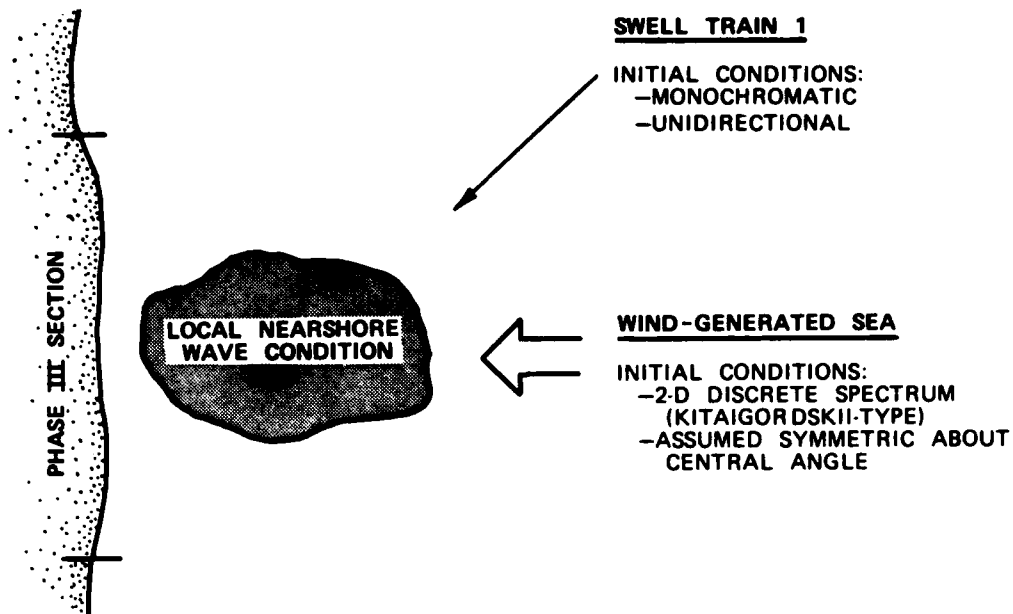


Figure 3. Generalized deepwater input conditions to the Phase III transformation technique

#### Processes Involved in Nearshore Wave Transformations

22. All of the processes that act on wave conditions during their transformation from deep to shallow water may be classified as to whether they are conservative or nonconservative. In conservative processes, any variations in spectral energies are due to redistribution of energy density rather than a loss (or gain) of energy out of (or into) the system. Except for continued wind input, all of the nonconservative processes for shoaling waves represent net sinks of energy. Thus, in almost all cases, there is a net loss of wave energy in waves propagating into shallow water.

### Conservative processes

23. Traditionally, the primary conservative processes considered in nearshore wave transformation have been refraction and shoaling. Models have been developed to treat these processes similar to the principles of geometric optics. Along a wave ray, the fundamental conservation law is given by

$$F_2(\underline{k}) = \text{constant} \quad (8)$$

where  $F_2$  is the two-dimensional wave spectrum in wave number ( $\underline{k}$ ) space. Transforming Equation 8 into frequency-direction space yields

$$E_2(f, \theta) c c_g = \left[ E_2(f, \theta) c c_g \right]_o \quad (9)$$

where  $c$  and  $c_g$  are the phase velocity and group velocity of the wave component, respectively, and the subscript "o" denotes deepwater conditions. Equation 9 states that in this space, the value of  $E_2(f, \theta) c c_g$  is always equal to its initial (deep water) value. Hence, as  $c$  and  $c_g$  change,  $E_2(f, \theta)$  must also change.

24. Using a straight parallel bottom assumption, a simple spectral model for refraction and shoaling can be developed. Since we are treating a relatively broad spectrum in the case of the local sea, linear wave theory should be quite adequate to model the various individual components. Hence,  $c$  and  $c_g$  are functions only of frequency and depth. This gives for the transformation of a given component

$$E_2(f, \theta) = \rho(f, h) \left[ E_2(f, \theta) \right]_o \quad (10)$$

where  $\rho(f, h)$  is defined as:

$$\rho(f, h) = \frac{(c c_g)_o}{c c_g}$$

25. It can be seen from Equation 10 that the energy density transformations are independent of approach angle. This may seem strange at

first since the refraction process is actually quite sensitive to initial wave angle. This paradox is resolved when a representation of the total energy is examined.

$$E_t = \int_0^{\infty} \int_0^{2\pi} E_2(f, \theta) d\theta df \quad (11)$$

which can be written in terms of the initial spectrum as

$$E_t = \int_0^{\infty} \int_0^{2\pi} [E_2(f, \theta)]_o \rho(f, h) \left| \frac{\partial \theta}{\partial \theta_o} \right| d\theta_o df_o \quad (12)$$

where  $\theta_o$  is used to denote the deepwater wave angle. This follows from Equation 11 since the frequency along a ray remains constant whereas the angle does not. The actual working limits of the integration about the directional distribution of  $E_2(f, \theta_o)$  are  $\pm\pi/2$  about the principal wave angle propagation normal to a given shoreline segment. All energy "outside" of this region propagates seaward and thus has no effect on the nearshore-wave climate.

26. From Snell's law, the shallow-water angle can be calculated as a function of frequency, depth, and the initial angle (Appendix B).

$$\theta(f, d, \theta_o) = \sin^{-1} \frac{c_o \sin \theta_o}{c} \quad (13)$$

It can be seen from Equations 12 and 13 that the effect of refraction is to compress the energy density into a successively narrower angle band as waves propagate toward a coast. Even though the energy density will remain high, the phase volume can significantly decrease for certain approach angles and, consequently, so can the total energy.

27. A numerical treatment of Equation 12 is very simple since  $\rho(f, h)$  and  $\left| \frac{\partial \theta}{\partial \theta_o} \right|$  are independent of energy density. They need be computed only once for a given set of frequency-direction increments and the total wave energy can be quickly calculated by an inner product formulation

$$E_t = \sum_j \sum_i E_{oi} \Lambda_{ij} \quad (14)$$

where  $i$  and  $j$  represent frequency and angle increments, respectively, and where  $\Lambda_{ij}$  represents a matrix of precomputed values of  $\rho(f, h)$  multiplied by  $\left| \frac{\partial \theta}{\partial \theta^q} \right|$ .

28. A second kind of conservative process consists of wave-wave interactions. These interactions are constrained such that:

$$\iint \frac{\partial F_2(k)}{\partial t} dk = 0 \quad (15)$$

$$\int \frac{\partial n(k)}{\partial t} dk = 0 \quad (16)$$

$$\int \frac{\partial E_1(f)}{\partial t} df = 0 \quad (17)$$

where  $n(k)$  is action density defined in terms of the wave number modulus  $k$ . Equations 15, 16, and 17 represent conservation of total momentum, total action, and total energy, respectively. These equations do not constrain these quantities to remain constant for a particular frequency direction wave component, however, since energy, momentum, and action can be interchanged among different components. Only the net integrals of the exchanges must be zero.

#### Nonconservative processes

29. Most theories of energy loss in shoaling waves have centered on wave-bottom interactions of a dissipative nature. Bottom friction, percolation, and viscoelastic effects have all been shown theoretically to be capable of removing significant amounts of energy from waves in shallow water (Hsiao 1978). Unfortunately, the empirical coefficients that are necessary when using these theories are quite dependent on sedimentary characteristics of the bottom over which the waves pass. This sensitivity would seem to suggest that significant variation of energy loss in shoaling waves might occur over relatively small time and

space scales. Furthermore, since these characteristics can change through time, no single transformation might be applicable at one site for all time.

30. In two recent studies (Goda 1974 and Battjes 1972), irregular wave breaking has been used to attempt to derive a rate of energy loss for waves near a coast. In both approaches, the probability of wave height exceeding some critical value is assumed to be governed by a modified Rayleigh distribution; however, what happens to the "broken" energy is treated differently in the two approaches. The observation of increases in whitecapping in shoaling waves and extensive surf zones with almost continuous wave breaking extending well offshore during storms are two supporting, albeit qualitative, pieces of evidence for this kind of wave breaking. The problem of estimating the energy loss described by Goda and Battjes is somewhat analogous to the problem of estimating energy losses in turbulence by following an individual eddy. To begin with, like the eddies, waves are a superposition of many interacting components; hence, if wave breaking occurs, there is considerable ambiguity as to which components are breaking. This closure problem makes it difficult to use the energy loss rates based on this approach with much confidence.

31. Recent studies by Heterich and Hasselmann (1980) and Shemdin et al. (1980) have shown that wave-wave interactions can create a strong flux of energy into high frequencies in shoaling waves. Although the wave-wave interactions are themselves conservative, this flux is into a region where the waves are unstable and wave breaking (or high viscous losses) can occur. The advantage of this approach to wave breaking is that the quantity predicted is the flux of energy into this unstable region and hence no information is required regarding the nature of the partitioning of "broken" and "unbroken" energy in individual waves. Nor is it necessary to reformulate a revised probability law of individual wave heights in shallow water.

32. The dominant transformation process in shallow water appears consistently to produce a similarity form for a spectrum (Kitaigordskii, Krasitskii, and Zaslavaskii 1975). In deep water, as seen in

Equations 3, 4, and 5, the wave spectrum follows an  $f^{-5}$  spectral shape in the region greater than  $f_m$ . In finite water depths, the general form is given by

$$E_1(f) = \frac{\alpha g^2 f^{-5}}{(2\pi)^4} \Phi(\omega_h) \quad (18)$$

where  $\Phi(\omega_h)$  is a nondimensional function varying from 1.0 in deep water to 0.0 when  $h = 0.0$ , as shown by Figure 4. When  $\omega_h$  is less than 1.0,  $\Phi(\omega_h)$  can be approximated by:

$$\Phi(\omega_h) \approx \frac{1}{2} \omega_h^2 \quad (19)$$

where

$$\omega_h = 2\pi f \left( \frac{h}{g} \right)^{1/2} \quad (20)$$

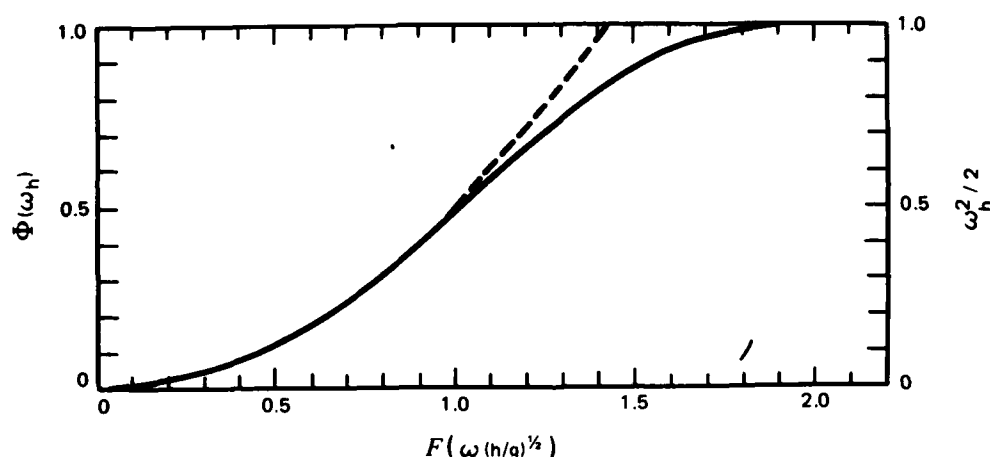


Figure 4. The functional relationships between  $\Phi(\omega_h)$  (solid line) and  $\omega_h^2/2$  versus  $(h/g)^{1/2}$  (from Kitaigordskii, Krasitskii, and Zaslavaskii 1975)

Replacing Equation 20 into Equation 18 will modify the spectral form to an  $f^{-3}$  shape or:

$$E(f) = \frac{\alpha g h}{8\pi^2} f^{-3} \quad f \geq f_m \quad (21)$$

In shallow water, the limiting spectral form is related to the water depth  $h$  and is proportional to an  $f^{-3}$  spectral shape. Studies by Goda (1974), Thornton (1977), Ou (1980), Iwata (1980), and Vincent (1981) support the form given by Equation 21. Employing Equation 21 as the shallow-water spectral shape assumes that  $\alpha$  remains constant from the wave conditions found in deep water. What has been found in prototype data is that  $\alpha$  varies with the "significant steepness" of the waves (based on  $H_s$ ) or the dimensionless peak wave number. Since bottom friction effects are ignored in the transformation effects, the assumption of a constant  $\alpha$  is not a bad approximation.\*

33. Since the geometry of the wave-wave interactions appears to force a constant spectral shape in wave number space, the ratio of momentum fluxes in various portions of the spectrum retains about the same relative values in both deep and shallow water. Sell and Hasselmann (1972) have shown that the relative values of the fluxes are (+1), (-4), and (+3) for the three lobes of the wave-wave interactions (Figure 5). Hence, during the entire time that the wave spectrum is adjusting from an  $f^{-5}$  to an  $f^{-3}$  shape, the majority of the momentum is going into higher frequencies where it is lost to turbulent and viscous dissipation. If the deepwater and shallow-water spectral forms are integrated, the total energies can be related to powers of the peak frequency. The ratio of the energies of the spectra can be defined as

$$R = \frac{E_o}{E_s} = \frac{g}{h} \omega_m^{-2} \quad (22)$$

where  $\omega_m$  is the radial frequency of the spectral peak ( $\omega_m = 2\pi f$ ). It should be understood that Equation 22 is only valid when the  $f^{-3}$  asymptotic spectral shape is attained in shallow water  $\left[ (h/g)^{1/2} \omega_m \leq 1.0 \right]$ ; otherwise the more general form

$$R = \tanh^2 k_m h \quad (23)$$

---

\* Personal communication, C. L. Vincent (1983), U. S. Army CERC, Fort Belvoir, Va.



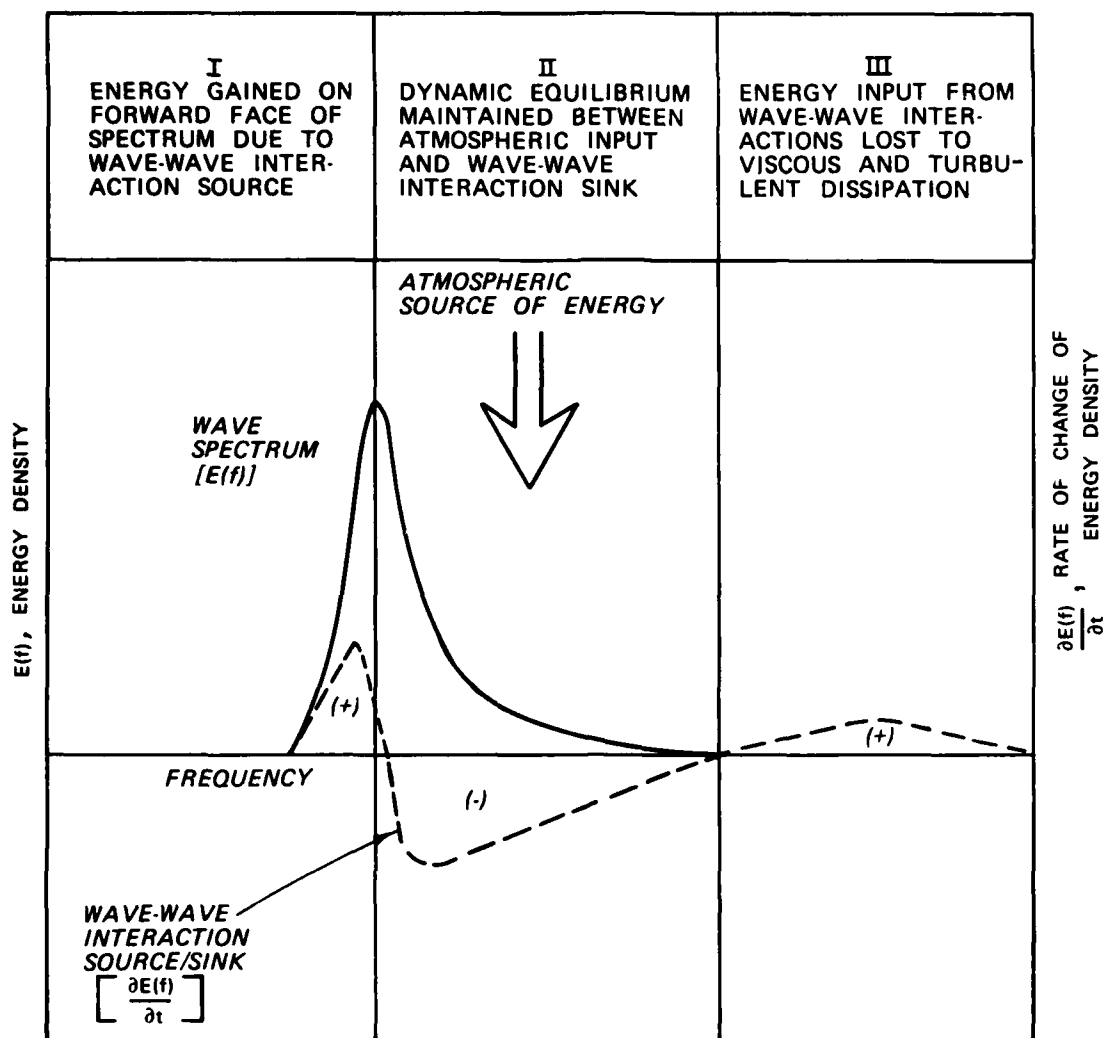


Figure 5. Schematic representation of the nonlinear wave-wave interactions

must be used. Equations 22 and 23 both assume that all of the energy transferred from the central portion of the spectrum is lost. One-quarter of the momentum is assumed to be transferred to the forward face of the spectrum where it should not be immediately lost. Relating the momentum to the energy in the spectrum will systematically estimate the amount of energy lost in these transformations. In shallow water the ratio of momentum to energy becomes

$$E = M\sqrt{gh}$$

where  $M$  is momentum; consequently this ratio is independent of frequency and one should expect that one-quarter of the energy transported out of the central portion of the spectrum is added to the energy on the forward face. Using this approximation, the net energy loss due to energy fluxes associated with wave-wave interactions is given by

$$E_L = \frac{3}{4} \left[ E_o - \tanh^2(k_m h) E_o \right] \quad (24)$$

and the remaining energy by

$$E_s = E_o \left[ \frac{1}{4} + \frac{3}{4} \tanh^2(k_m h) \right] \quad (25)$$

34. Equation 25 should provide a good approximation to the energy loss in a shoaling spectrum due to the expected change in spectral shape as long as the spectral peak remains at about the same frequency. As the spectral peak migrates into lower frequencies, the region of energy loss will extend into these frequencies and Equation 25 will underpredict the amount of energy loss. Also, it should be borne in mind that Equation 25 has neglected all additional energy loss mechanisms such as the wave bottom interactions mentioned previously. Thus Equation 25 is expected to provide a reasonable, slightly conservative approximation to the wave energy remaining in shallow water. Field evidence supporting the dominance of energy loss in shallow water due to this single mechanism, along with a more detailed theoretical treatment, can be found in Vincent (1981).

35. One significant unresolved problem still remains in the general treatment of the Phase III data, due primarily to the assumption of straight parallel offshore contours. As illustrated in Figure 6, sheltering effects associated with the geometry of the coastline can introduce significant deviations from the results derived from a straight coast approximation. The solution to the sheltering problem is straightforward for both sea and swell wave conditions. Sea wave conditions are described by a two-dimensional discrete spectrum  $(E_{o_{ij}})$ . A function can

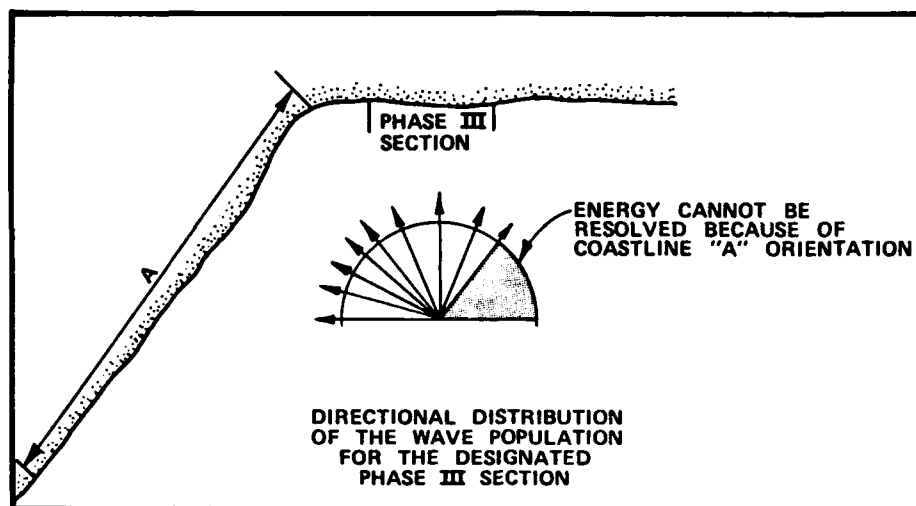


Figure 6. Generalization of spectral and wave sheltering

be introduced into Equation 14 that allows only certain angle bands in the two-dimensional spectrum to arrive into a sheltered coastal reach; thus the total energy can be expressed as

$$E_T = \sum_j \sum_i E_{o_{ij}} \Lambda'_{ij} \quad (26)$$

where  $\Lambda'_{ij}$  is defined as

$$\Lambda'_{ij} = \Lambda_{ij} \Delta_j$$

where  $\Delta_j = 1$  for wave angles that can arrive at the coast and  $\Delta_j = 0$  for wave angles that are prevented from reaching the sheltered section of the coast. Swell wave conditions are assumed to be described as unidirectional monochromatic waves; thus any waves propagating from a sheltered area are set to zero.

36. The amount of wave sheltering (or the selection of a sheltering angle) depends on the location of the input Phase II station (Plates 1-6) relative to the Phase III station being considered. Also, one must consider the location of the land boundary points within the Phase II grid relative to the actual shoreline. There is a limited amount of subjectivity involved in the selection of sheltering angles

when all of the above variables are accounted for.

37. In very shallow water, it is expected that the similarity process governing the equilibrium range  $k^{-3}$  form must eventually break down as wave breaking begins to occur at frequencies near the spectral peak. At that point, the spectrum may evolve to a different shape than that given by Equation 21. However, evidence from a study by Vincent (1981) suggests that the nearshore energy still behaves in a manner consistent with the equation. The integrated form of Equation 21, which predicted a dependence of the wave height on the square root of depth, provides much better agreement with observed wave heights. Therefore, in shallow water, the following equation can be used to describe the variation of wave height with depth

$$H_{se_{max}} = \frac{\sqrt{\alpha g h}}{\pi} f_c^{-1} \quad (27)$$

where  $\alpha$  is the Phillip's equilibrium constant,

$$f_c = 0.9 f_m \quad (28)$$

and  $f_c$  is defined as a cutoff frequency. This equation may be used to limit the locally generated sea wave height found in the Phase III wave data without having to rely on a single limiting breaking wave condition. This has the advantage that all of the wave heights exceeding a critical value at some depth are not mapped into the same nearshore wave height.

38. Although recent field evidence appears to support an  $H \sim h^{1/2}$  relationship in very shallow water for broad spectra, there is a substantial set of theoretical and laboratory studies that support a linear relationship between monochromatic wave height and depth (employed for the swell breaking limit),

$$H_{sw_{max}} = \epsilon h \quad (29)$$

where  $\epsilon$  is a dimensionless constant with a value generally around 0.8. Thus there is a fundamental difference between spectral and monochromatic forms of wave breaking in shallow water. The ability to treat the local sea and the swell wave trains separately is consequently a necessary element of the Phase III methodology.

39. Figure 7 presents a schematic interpretation of the overall Phase III methodology as developed in this section. Two independently specified wave trains, each represented by an appropriate set of parameters, are transformed into shallow water. This separation allows the treatment of the transformation process to be specified differently for each wave train. Since averaging of wave approach angles is not always reasonable and since different mechanisms appear to be important in broad and narrow (monochromatic) spectra, this approach permits the transformation process to be properly posed for each wave train.

#### Comparisons

40. Comparisons to actual gage measurements are necessary to determine the validity of the long-term wave statistics presented in WIS Report 9 (Jensen 1983). Phase III wave data were computed for 166 station locations along the Atlantic coast (every 3 hr for the 20 years from 1956 through 1975). Measured wave data were obtained at various locations along the Atlantic coast from the wave measurement program of the Coastal Engineering Research Center (Thompson 1977).

41. Table 1 shows the latitude and longitude of the locations at which measurements are available and the corresponding Phase III station locations. Additional information concerning the type of wave gage used and water depth at the gaging site is included. It must be emphasized that all gage measurements are highly dependent on located conditions such as water depth, bottom topography, temporal changes in bottom topography, and pier effects. These physical conditions are considered as subscale features in comparison with the Phase III shoreline sections (10 miles\*) and are neglected in the hindcast data.

---

\* To convert miles to kilometres, multiply by 1.609344.

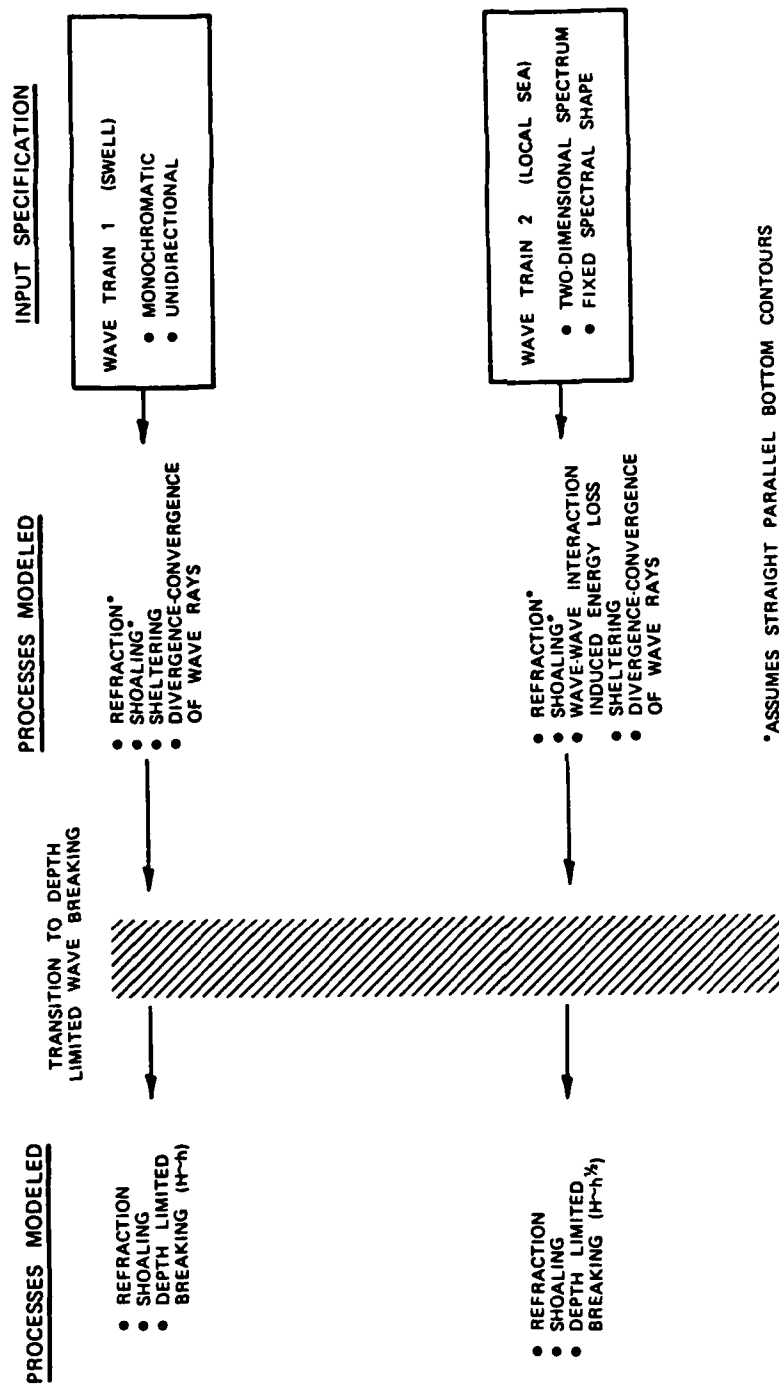


Figure 7. Schematic of the methodology associated with the Phase III transformation technique

42. The Phase III wave data are paired as closely as possible to the measured data. This assumes that the gage data (given in observation number per day or four observations per day) are recorded at 6-hr intervals (0000, 0600, 1200, 1800 hours). There will be a slight phase shift in the two data sets caused by the assumption that wave conditions generated via the Phase III methodology neglect propagation time from deep to shallow water.

WIS Phase III  
hindcast wave data

43. For the comparisons in this report, computed wave heights are determined from the combined energy associated with both sea and swell wave populations, or  $H_s = \sqrt{H_{SEA}^2 + H_{SWELL}^2}$ . The peak period wave information presented is derived from the selection of the sea or swell peak period containing the dominant wave energy. The mean directions of wave propagation are also provided for sea and swell wave populations, but are not used because no measured wave data contain directional information.

Measured wave data

44. The Coastal Engineering Research Center (and its predecessor, the Beach Erosion Board) has operated wave gages in the nearshore area for more than 30 years. Recent wave data have been analyzed and tabulated (Thompson 1977). The measured gage data employed in all comparisons are derived from this work. Three different wave recording devices (step-resistance, continuous wire, and pressure-sensitive) were used at the various gage sites and are shown in Table 1. The approximate gage locations also are shown in Figure 8. These gages have been shown to respond differently to identical wave conditions (Thompson 1977). Step-resistance wave gage results were found to be approximately 1 ft higher for low wave conditions and 20 percent higher for high wave conditions in comparison with continuous wire and pressure-sensitive gages. This will produce individual bias in the resulting wave data.

45. The wave data obtained from all pressure-type gages are based on a theoretically derived expression relating the measured dynamic pressure to the free surface oscillations. The basic problem encountered

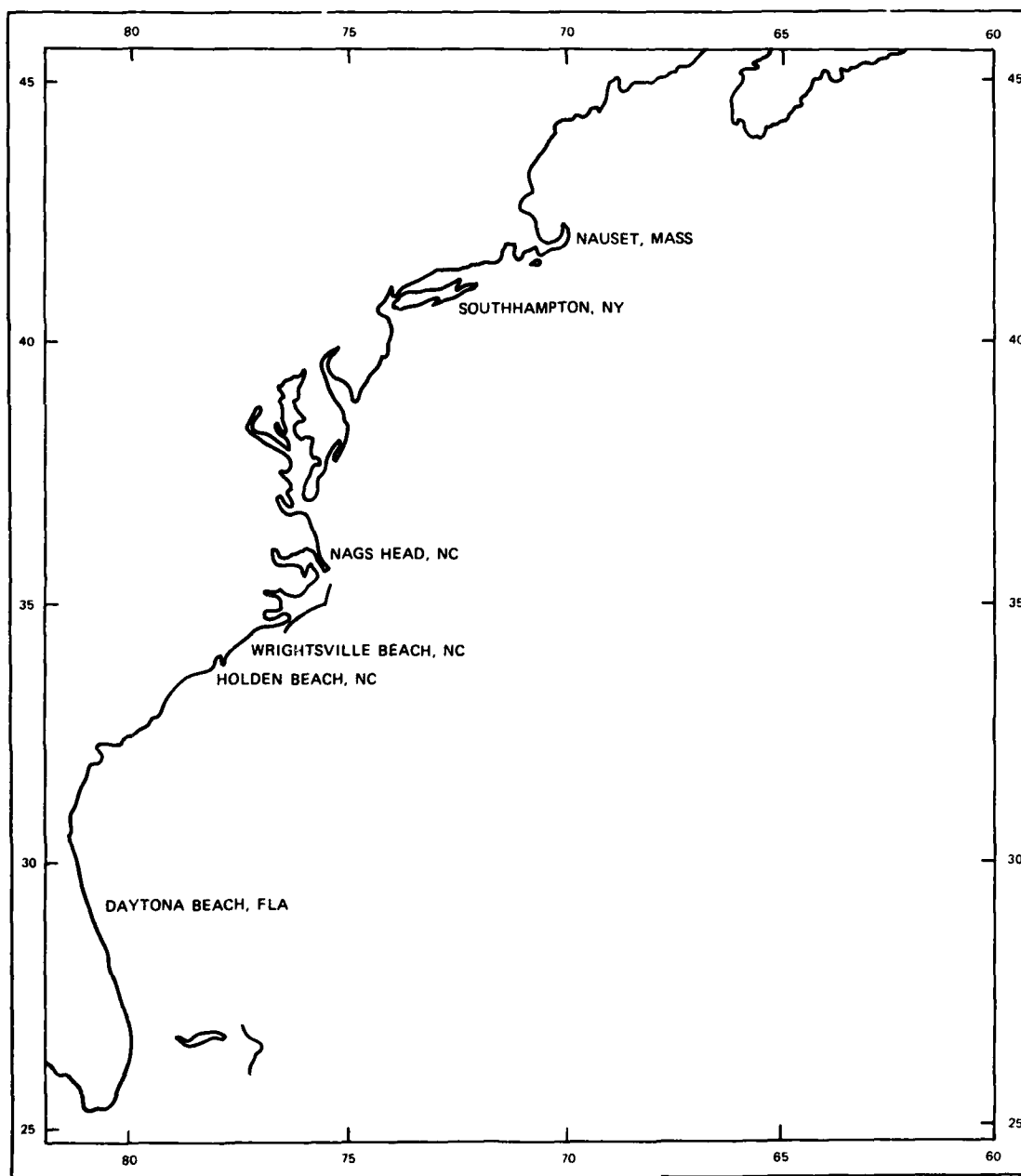


Figure 8. Approximate location of wave comparison sites



was how to compensate for the pressure signal attenuation due to gage submergence. Generally, this relationship is based on linear wave theory where a simplified transfer function acts as a multiplier to change a pressure spectrum to a free surface spectrum. This transformation caused many problems in the analysis of the wave data obtained from all pressure gages and should be identified at the onset of this discussion. Due to its sensitivity, the accuracy of the  $H_s$  derived from the pressure gages may be questioned (Thompson\*).

46. All summary wave data ( $H_s$  and  $T_p$ ) were generated from digital wave records and analyzed in a similar fashion. The significant height is equal to four times the standard deviation of record, and  $T_p$  is equal to the frequency at which the maximum energy density exists. The analysis of the wave record employs a constant frequency interval such that converting wave frequencies to wave periods will result in a bias toward 8- to 9-sec peak wave periods in comparison to 7- to 8- and 9- to 10-sec peak periods (Thompson 1977).

47. Variations in water depths at the gage location also will influence the measured wave conditions. The bottom topography in a near-shore area will change over time such that depth-limiting wave conditions will also vary. Changes in wave conditions from 10 m (water depth for Phase III data) to 7.6, 5.2, 4.6, and 3.3 m (water depths at wave recorders, as shown in Table 1) could be dramatic. Wave refraction and shoaling will either amplify or attenuate wave heights as much as 25 percent. Also, the nonlinear energy transfers play an important role in the nearshore region, affecting both the  $H_s$  and  $T_p$  result (Vincent 1982). One also must consider the effects of wave breaking, on a wave-to-wave basis, within a given wave record and also the overall collapse of the spectrum in very shallow water or when extreme wave conditions prevail.

48. There is also a certain degree of uncertainty associated with gage records containing no data for a given observation. It is not

---

\* Personal communication, E. F. Thompson (1983), U. S. Army CERC, Fort Belvoir, Va.

known whether a malfunction in the recorder or analysis did not permit the computation of the wave parameters ( $H_s$  and  $T_p$ ), or if special computations were not made because the significant wave heights (derived from evaluating the standard deviation of the wave record) were less than 0.4 ft (Thompson 1977). This uncertainty would lead to a bias in the measured data toward a higher percentage of large wave heights, or omitting wave conditions less than 0.4 ft (although these conditions were considered to be rare).

49. Thus the comparisons presented in this section are not absolute because of the differences in physical constraints associated with the gaging and hindcasting locations. They will show how accurately (with the given differences) the hindcast data represent the nearshore wave climate.

50. Simple yet descriptive techniques were employed for the comparisons: time series plots, cross plots, and percent occurrence tables and plots. The last of these types of comparisons is probably the most indicative of the ability of the hindcast wave data to represent a wave climate accurately. The two data sets were paired according to the gage observation. These paired-data techniques are used to describe the random error of the hindcast model. However, much of the random error in these computations is attributed to shifts in time between the wave hindcasts and observed wave height. Consequently, for the evaluation of these hindcast data relative to wave climate representations, major emphasis is centered on the long-term comparisons of means and probability distributions in which the time factor has been removed.

#### Time-history comparisons

51. Although the time-history comparisons shown in Appendix C do not provide a numerical value for difference or similarity, they are qualitative descriptors of the random error of the hindcasting technique. In general, all of the time series plots show that the hindcast  $H_s$  is distributed through time similar to the distribution of the measured  $H_s$  (Figures C1-C16). Some intervals show the computed waves to be "out-of-phase" with respect to the measured data. This out-of-phase characteristic can be attributed to the Phase III methodology, in that

propagation of wave conditions from the Phase II wave data to the Phase III station location is not considered.

52. The first set of time-history plots (Figures C1-C3) represent comparisons from the Nauset gage site. Six events are displayed in these figures and are well represented by the hindcast data. Wave growth over time in the hindcast data is very similar to that displayed in the gage results for all six events. The peak wave conditions near 9 December 1974 are amplified in the hindcast results in comparison with the gage data, whereas during 15-18 December 1974, the hindcast data display lower maximum conditions over the gage results. The reasons for these dissimilarities can be attributed to the gage monitoring highly site-specific conditions which the hindcasting technique was not designed to do.

53. The second set of time-history plots shows comparisons of gage and hindcast results at Southhampton (Figures C4 and C5). There are slight phase shifts between the two data sets, but in general the hindcast data follow the wave condition trends found in the gage results. Two interesting results are shown in these plots. The first shows that the gage results are not continuous. Malfunctions in the recorder or analysis cause gaps in the results. For the five storm events shown in Figures C4 and C5, only one storm event reaches a maximum condition (25 November 1975). When data are missing from a continuous record period, a certain amount of bias is introduced in the overall statistical distributions for the given location. The second point that must be noted is that during periods of low wave energy conditions, the Phase III hindcast data will become very calm (i.e.  $H_s$  approaches 0.0), whereas the gage records larger results. These differences could be attributed to (a) generation of wave energy in the nearshore area which the gage records but the hindcast assumes to be negligible, (b) background noise either in the high or low frequency end of the spectrum which was carried through the analysis, or (c) a result of the physical geometry of the given gage site.

54. The third set of time-history plots presents comparisons of gage and hindcast results at Nags Head (Figures C6-C8). The peak wave

periods ( $T_p = 1/f_m$ ) derived from the gage and hindcast results also are displayed. The  $H_s$  results clearly show that the hindcast accurately represents storm event conditions. The growth and decay of the near-shore wave conditions are also adequately described. The peak period results display dissimilar trends between the gage and hindcast data sets. The primary reason for the differences are caused by the gage recording a multicomponent (in frequency) wave system, whereas the hindcast data are represented by a two-component system (sea and swell). Also, the one-dimensional frequency spectrum derived from the gage record contains 89 frequency bands (at a constant interval), whereas the hindcast spectrum is modeled with 20 frequency bands (at variable frequency intervals) (Resio 1981). Thus the declaration of the peak period results obtained from the gage analysis would show larger changes from observation to observation.

55. Three additional sets of time-history  $H_s$  results are shown in Figures C9-C16 for Wrightsville Beach, Holden Beach, and Daytona Beach. The trends in the hindcast data are in agreement with the gage results. Because of the difference in water depths (10 m for the hindcast data and 5.18, 4.57, and 3.35 m for Wrightsville, Holden, and Daytona Beach data, respectively), the hindcast  $H_s$  for maximum conditions generally overpredicts the gage data because of depth-limited wave breaking, whereas during moderate to low wave conditions the differences between the two data sets are minimal. Even slight variations in the wave climate represented in the gage record (Figure C14, from Daytona Beach) are very closely approximated in hindcast data.

#### Percent occurrence comparisons

56. There is a degree of uncertainty associated with the statistical representations of the wave climate at a given location. One must be aware that even the gage cannot uniquely describe actual wave conditions during a given sampling period. Use of long-term, continuous (defined here as a constant number of observations per day over a prolonged period of time)  $H_s$  and  $T_p$  data will offset the inconsistency in the actual and measured wave conditions. Unfortunately, the longest measured wave data set is from Nags Head, North Carolina (spanning 7 years

with a total of 4,492  $H_s$  and  $T_p$  observations). This means that 4,268 observations are either calm (defined by Thompson 1977) or missing. The working data set only contains approximately one-half of the total expected number of observations. Thus a bias of unknown quantity is introduced into the gage results because of the noncontinuous data set. The hindcast data presented in the percent occurrence plots also will be biased because they are paired as closely as possible to the gage data through time. Hence, any differences found in these comparisons will be caused by the hindcast's own bias. The percent occurrence in the  $H_s$  data will also be influenced by the water depth differences between the hindcast results (10 m) and the gage results (9.76, 5.18, 4.57, and 3.35 m). All wave conditions will be subject to the effects of wave shoaling from 10 m to the gage water depth where increases as much as 25 percent can be expected based on theoretical considerations. Wave refraction can diminish the effects of wave shoaling, but under certain conditions an increase in wave height can be expected.

57. For each site, the percent occurrence for  $H_s$  and  $T_p$  is compared. The paired data (hindcast and gage results) are separated into  $H_s$  intervals of 0.5 m and the  $T_p$  in intervals of 1.0 sec. These plots are generated for comparison purposes only and should not be construed as the representative wave climate expected for that specified location.

58. Figure 9 displays the percent occurrence of  $H_s$  and  $T_p$  conditions for Nauset Beach, Massachusetts, from 1974-1975. The wave recorder is a pressure gage mounted approximately 10 m below the mean water level. The hindcast  $H_s$  results are shown to underpredict the gage results in all but the first category. The difference in the percent occurrence for large wave conditions could be attributed to the greater water depth found at the gage location. The reason for the large difference in the first two categories (<0.5 m and <1.0 m) cannot be explained at this time. The tail of the percent occurrence (for wave conditions from <2.0 to <5.0 m) shows that the hindcast varies from the gage results by 4 percent at its maximum. The percent occurrence in the measured  $T_p$  results demonstrates that there is a bias away from wave

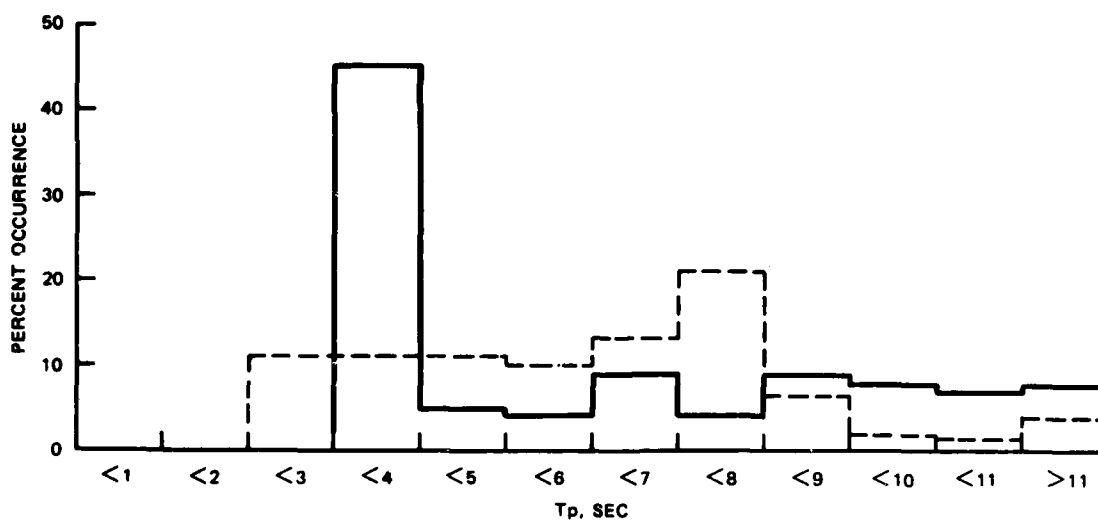
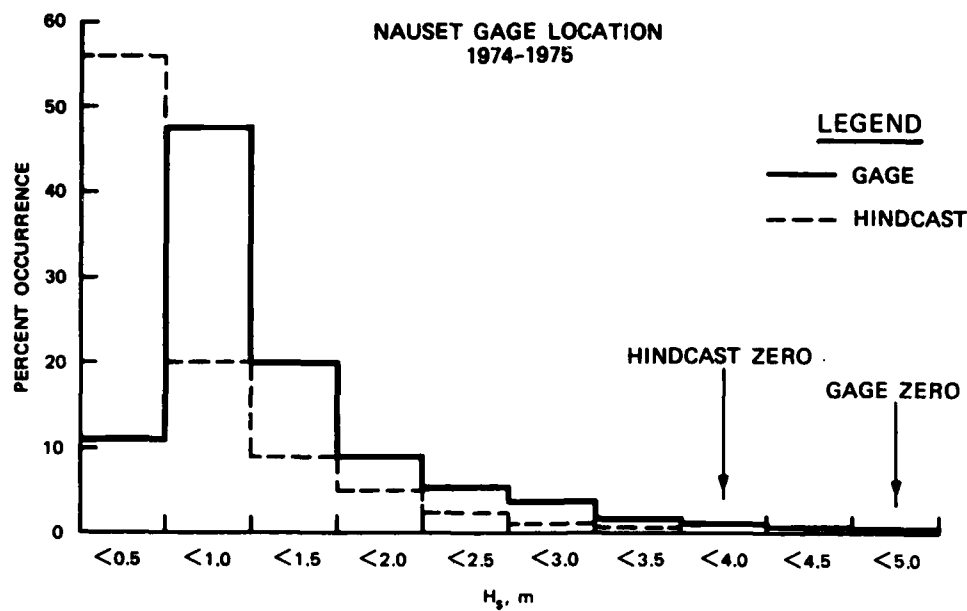


Figure 9. Percent occurrence versus  $H_s$  and  $T_p$  for time-paired (997 observations) measured and computed data sets at Nauset, Mass.

periods in the category  $<8$  sec. There is also a large portion (45 percent) of wave conditions with  $T_p$  values  $<4$  sec. By linear theory, wave frequencies greater than 0.27 Hz should not be resolvable in a water depth of 10 m. There appears to be some question as to the validity of all results with  $T_p$  values less than 3.7 sec. There were problems associated with initial measurements taken at Nauset Beach (as previously mentioned, paragraph 45) that would result in inconsistent wave conditions. Rather than edit the measured data by theoretically derived limiting conditions, it was felt that the gage results should be presented in untampered form.

59. The second location for comparisons is the Southhampton, New York, gage site. The gage is a pressure type gage located in approximately 10 m of water. The percent occurrence of  $H_s$  and  $T_p$  is shown in Figure 10. The hindcast results compare extremely well with the gage results in terms of the  $H_s$  data. The maximum difference is approximately 8 percent while, in general, differences of approximately 2 percent exist throughout the distribution. The maximum difference in the  $T_p$  results is approximately 10 percent found in the gage biased category  $<8$  sec.

60. The third gage location for comparisons is at Nags Head, North Carolina (Figure 11). Two types of monitoring devices were employed. A step-resistance gage (from 1968-1972) and a continuous wire gage (from 1972-1975). The differences found in the percent occurrence plot for the  $H_s$  categories  $<0.5$  and  $<1.0$  m can be attributed to the bias associated with the step-resistance gage (measuring approximately 0.3 m high for low wave conditions). If this "error" were used to compensate the gage data, then the differences between the hindcast and gage data would be approximately 10 percent. The percent occurrence distribution for larger wave conditions shows differences of 5 percent (at the maximum) between the two data sets. Because of the differences in the water depth where the wave information is generated (10 m for the hindcast results and 5.18 m for the gage results), there will be slight dissimilarities in the extremely large wave heights. One possible cause for the difference could be the difference in the techniques used in the

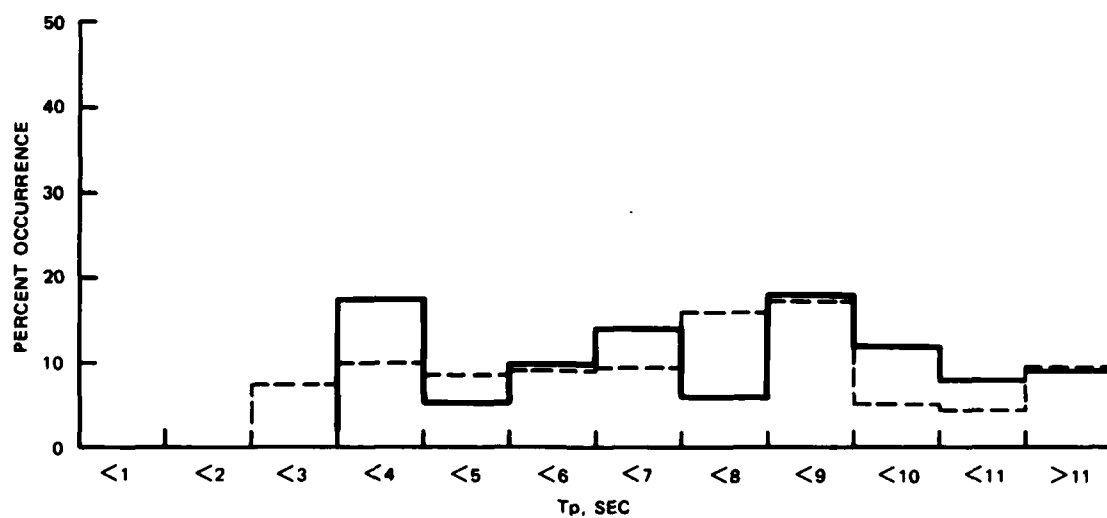
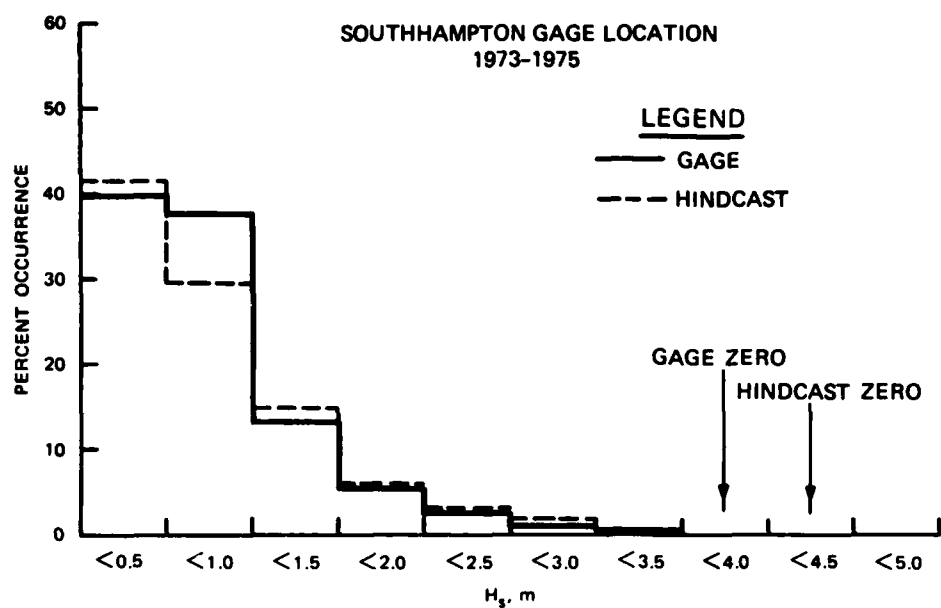


Figure 10. Percent occurrence versus  $H_s$  and  $T_p$  for time-paired (1352 observations) measured and computed data sets at Southampton, New York



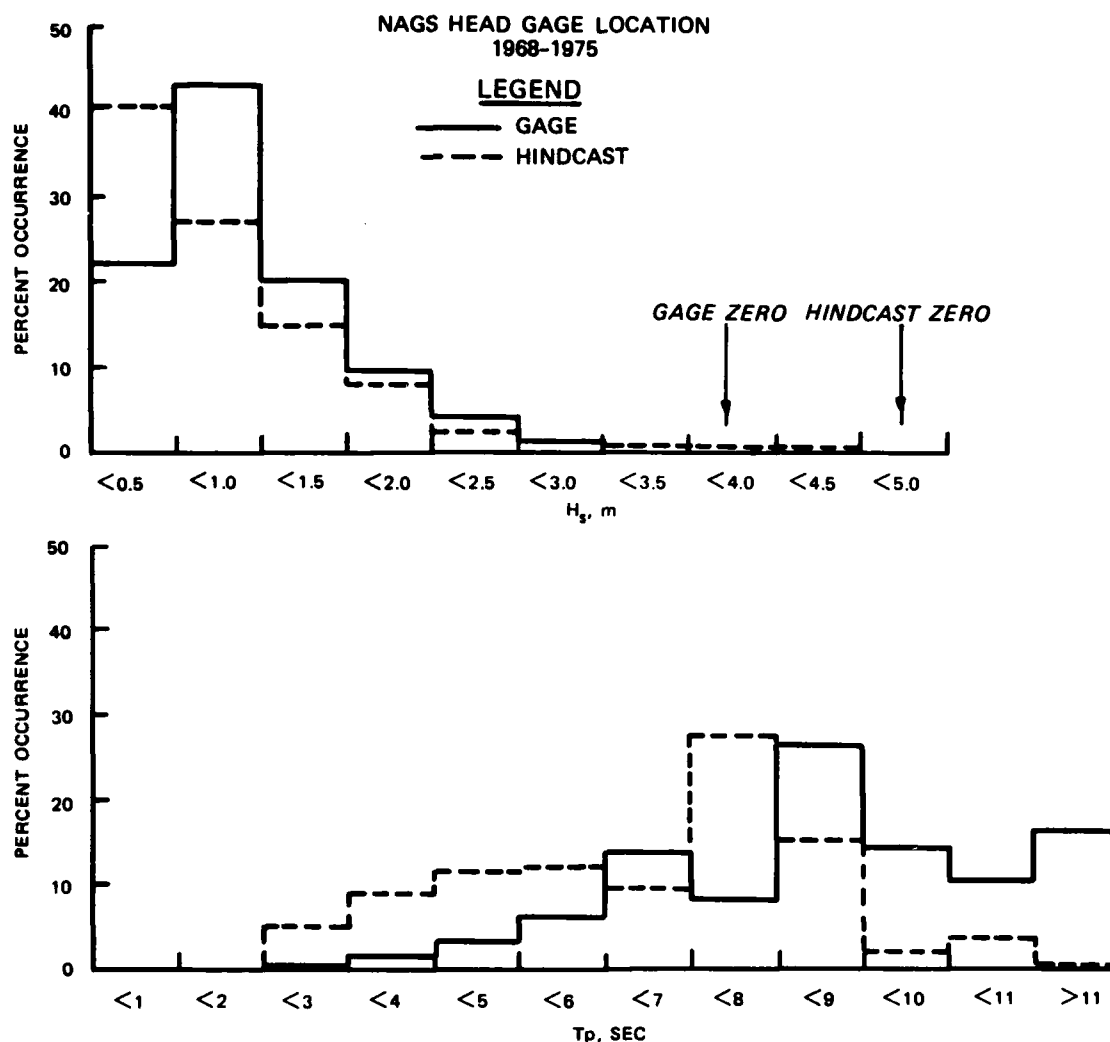


Figure 11. Percent occurrence versus  $H_s$  and  $T_p$  for time-paired (4492 observations) measured and computed data sets at Nags Head, North Carolina

assignment of peak period in the gage hindcast analyses. In Figure C6, the gage records indicate a shift in period from  $\sim 3$  sec to  $\sim 14$  sec while the wave height remained almost constant. Shifts in wave period, as those shown in Figure C6, are considered to be unrealistic, and for wave heights of 0.2 to 0.4 m, relatively unimportant. In Figure C8, the gage recorded period shifts from  $\sim 9$  sec to  $\sim 4$  sec within one recorded interval while the wave height was increasing slightly. Again, this shift is

not realistic; and the hindcast representation is more appropriate. Also, the differences in the  $T_p$  results could be caused by the input, deepwater wave information. The hindcast model (Resio 1981) tends to "wash-out" long-period low-amplitude swell where the energy is numerically dispersed throughout the grid.

61. The statistical distribution comparisons for  $H_s$  and  $T_p$  at Wrightsville Beach, North Carolina, are presented in Figure 12. At this location, two wave gaging systems were employed (a step-resistance type, from 1970 to 1974, and a continuous wire type, from 1975 thereon). Again the two data sets compare favorably for  $H_s$  conditions from  $<1.5$  m to their extreme, while the bias in the step-resistance gage (1.0 ft for low wave conditions) produces the differences found in the  $<0.5$  and  $<1.0$  m height increments. If the bias in the gage data is corrected, the difference between the two data sets is 20 percent in wave-height classes  $<0.5$  and  $<1.0$  m. Although this difference is very large, the total percent occurrence of wave conditions in both categories differs by only 4 percent. Similar inconsistencies are found in the  $T_p$  distributions as were previously found in the Nags Head data.

62. The Holden Beach, North Carolina, and Daytona Beach, Florida, percent occurrence plots are displayed in Figures 13 and 14. The water depths at the gage location are 4.57 and 3.35 m, respectively, and the wave monitoring devices for these locations were continuous wire type (Holden Beach) and pressure type (Daytona Beach). Again, under low wave conditions the hindcast produces a larger percentage of  $H_s < 0.5$  m while the gage results show a larger percentage of  $H_s < 1.0$  m. The differences between the two sets of data are approximately 15 percent at their maximum. Comparing the percent occurrence of  $T_p$  derived from the hindcast and gage data one finds good agreement at Holden Beach for nearly all wave period categories (with exception of the biased  $<8$  sec category of the gage data). At Daytona Beach the gage results show a higher percentage of long wave periods whereas the hindcast data consist of a higher percentage of shorter period wave conditions.

#### Extreme storm event comparisons

63. A final comparison is made between extreme storm wave

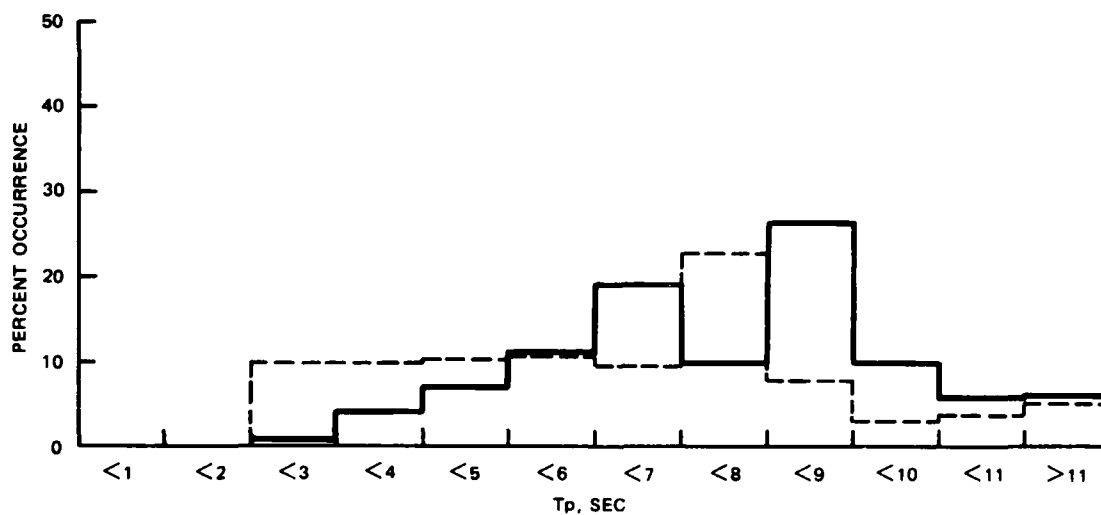
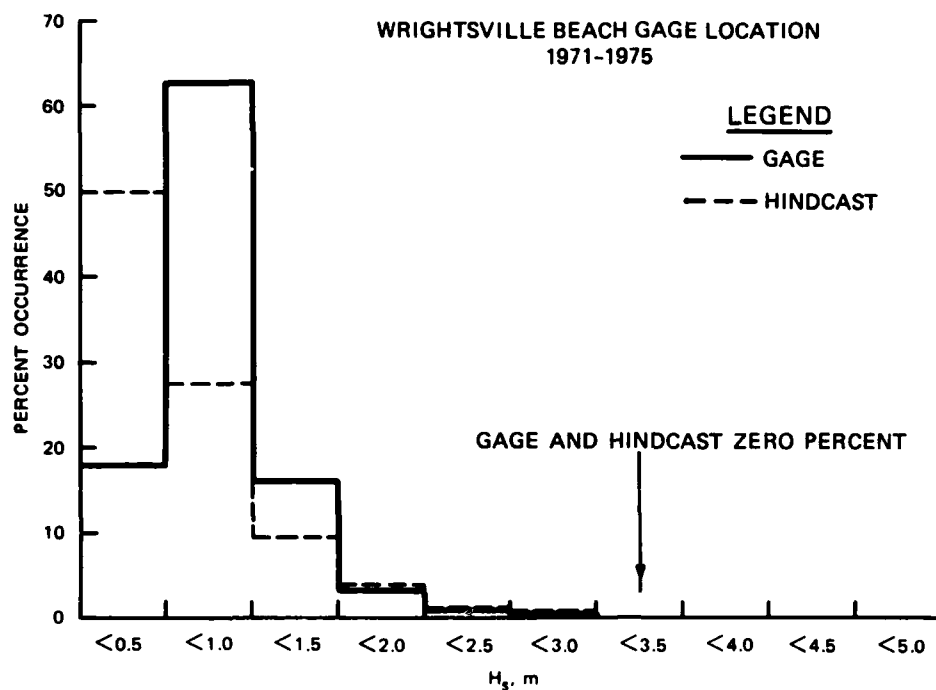


Figure 12. Percent occurrence versus  $H_s$  and  $T_p$  for time-paired (4126 observations) measured and computed data sets at Wrightsville Beach, North Carolina

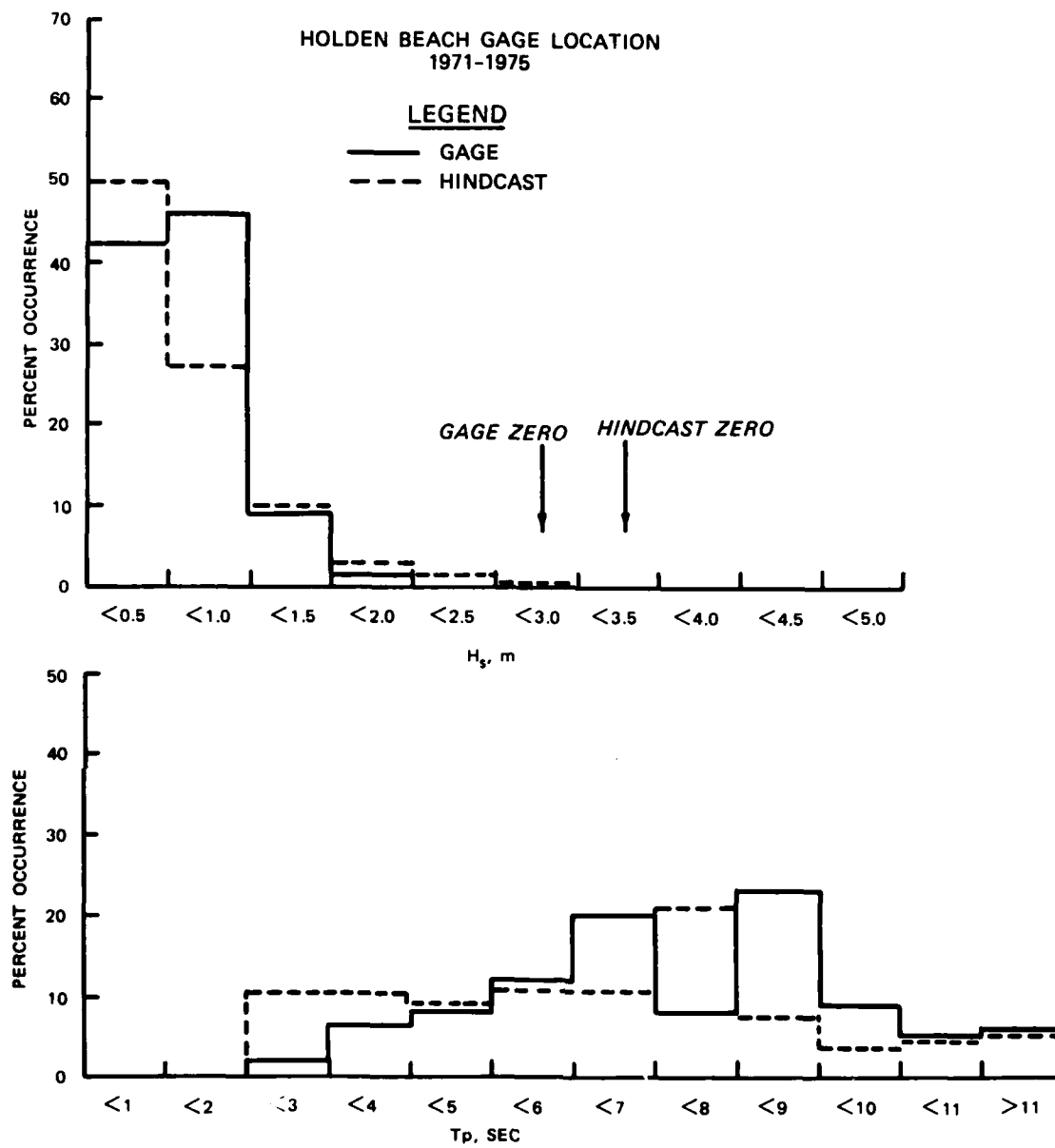


Figure 13. Percent occurrence versus  $H_s$  and  $T_p$  for time-paired (3249 observations) measured and computed data sets at Holden Beach, North Carolina

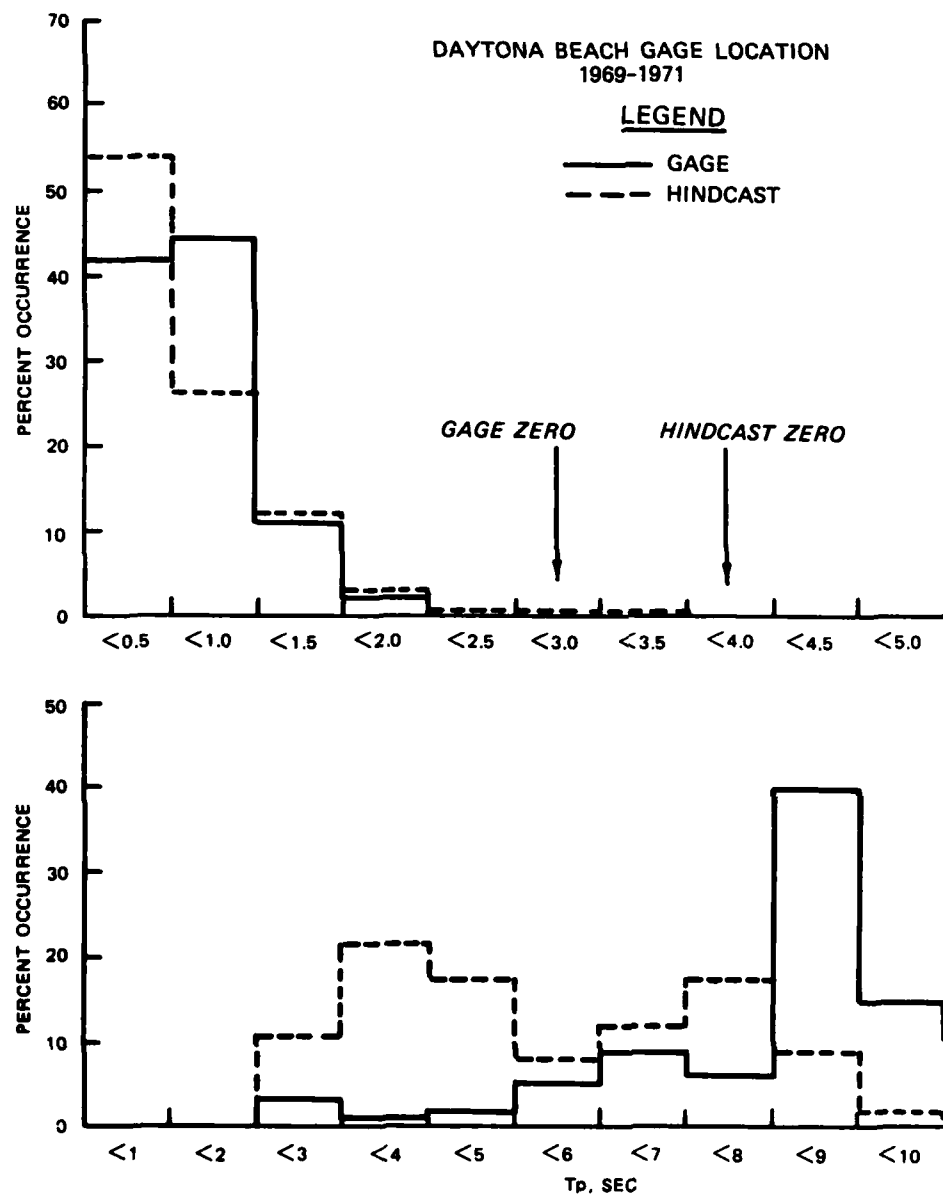


Figure 14. Percent occurrence versus  $H_s$  and  $T_p$  for time-paired (1011 observations) measured and computed data sets at Daytona Beach, Florida

conditions. The data were derived by selecting the top 20 to 30 storm events within the gage sampling period. The maximum  $H_s$  from that event was recovered. The date of these events then was used to scan the hindcast data set to select the maximum  $H_s$  from the storm. These maximum  $H_s$  conditions are not identically paired in time (lag time caused by nonpropagation of wave conditions from the Phase II input conditions) but are representative of the event. In some instances, the water depth at the gage site will greatly influence the maximum wave conditions. These data will be biased toward lower  $H_s$  results for a particular storm condition in comparison to the hindcast results.

64. The Nauset, Massachusetts, gage site extreme  $H_s$  conditions are compared with the hindcast results shown in Figure 15. For  $H_s$  conditions up to approximately 2.5 m, the hindcast results generally tend to be slightly underpredictive to the gage data. Above this point, the gage results are shown to be from 1.0 to 2.0 m higher for maximum wave

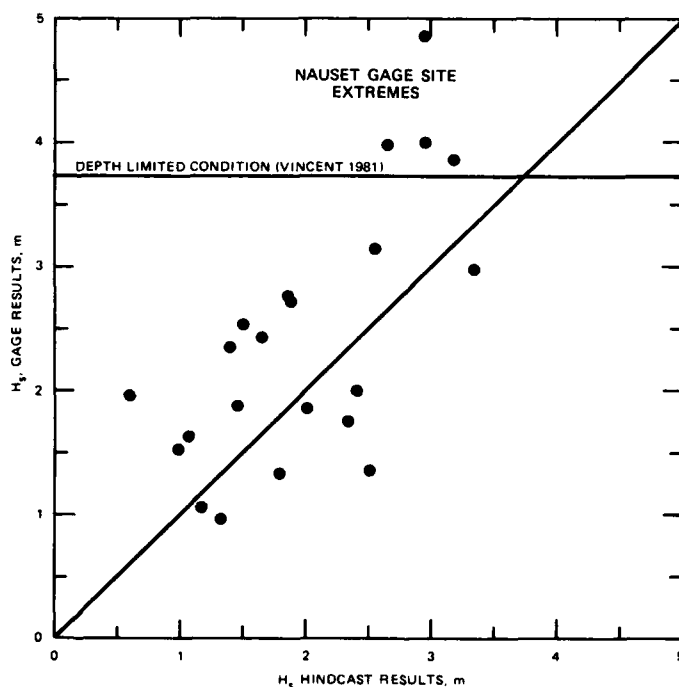


Figure 15. Cross plot of measured ( $h = 10.7$  m) and computed ( $h = 10$  m) maximum  $H_s$  conditions occurring in a specific event for Nauset, Mass.

conditions in comparison with the hindcast results. From this data set, only one storm event was completely missed by the hindcast ( $H_s \approx 2.0$  and  $H_s^{\text{HINDCAST}} \approx 0.6$  m); all other events were found in the hindcast data set.

65. The plot of extreme storm conditions for Southhampton is displayed in Figure 16. These data show that the hindcast results are underpredictive for low wave conditions (less than approximately 2.0 m), then tending toward overpredicting  $H_s$  results greater than 2.5 m. There is no apparent reason for these differences.

66. The final four figures (Figures 17-20) are comparisons of the extreme wave conditions for Nags Head, Wrightsville Beach, Holden Beach, and Daytona Beach. All gage results are highly dependent on the water depth at the gage sites (5.18, 5.18, 4.57, and 3.35 m, respectively) and become biased toward lower  $H_s$  values in comparison with the hindcast results and tend to underpredict the gage results. Above this point, the hindcast results (being in deeper water) tend to overpredict the measured data. In these comparisons there is only a limited number of storm events completely missed by the hindcast, the maximum number occurring at the Wrightsville Beach gage site.

### Summary and Conclusions

67. The methodology of the Phase III portion of the Wave Information Study has been summarized and comparisons have been made to six unique gage locations along the Atlantic coast. The transformation matrix operator generating the hindcast wave data remained constant from one gaging site to the next. Only variations in the first-order approximation to the shoreline orientation (wave generating model) slightly change the generalized transformation matrix operator.

68. There are areas along the Atlantic coast where the Phase III wave data (WIS Report 9, Jensen 1983) may not be appropriate. Since wave conditions are not measured along the total length of the Atlantic coast, all Phase III station data cannot be verified. The whole coast of Maine presents a significant problem in the declaration of 10-mile

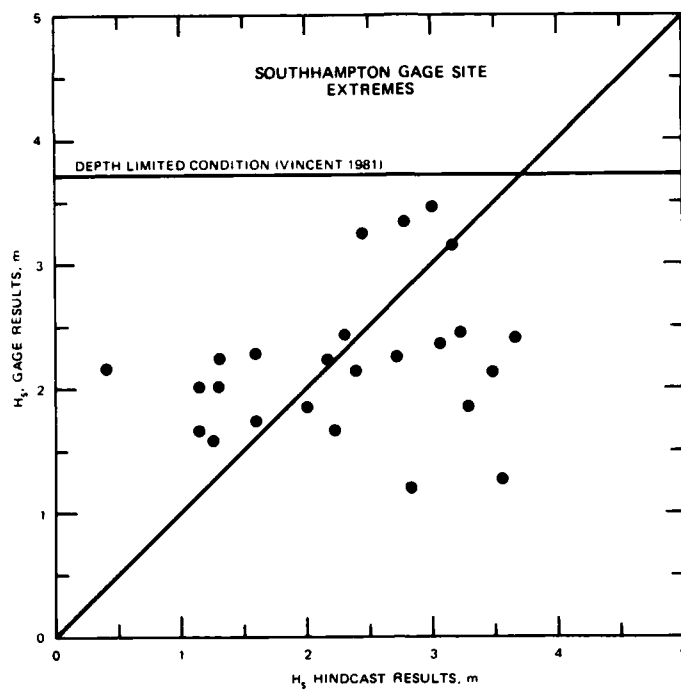


Figure 16. Cross plot of measured ( $h = 9.8$  m) and computed ( $h = 10$  m) maximum  $H_s$  conditions occurring in a specific event for Southhampton, New York

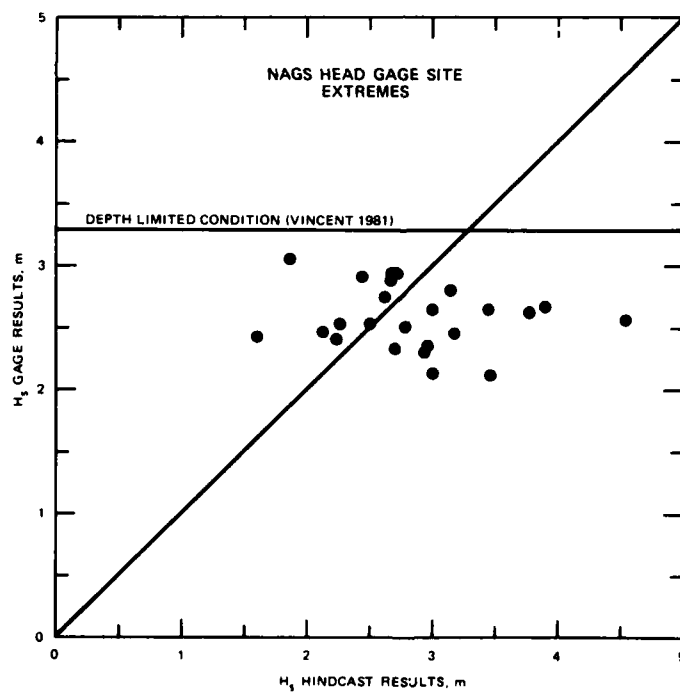


Figure 17. Cross plot of measured ( $h = 5.2$  m) and computed ( $h = 10$  m) maximum  $H_s$  conditions occurring in a specific event for Nags Head, North Carolina



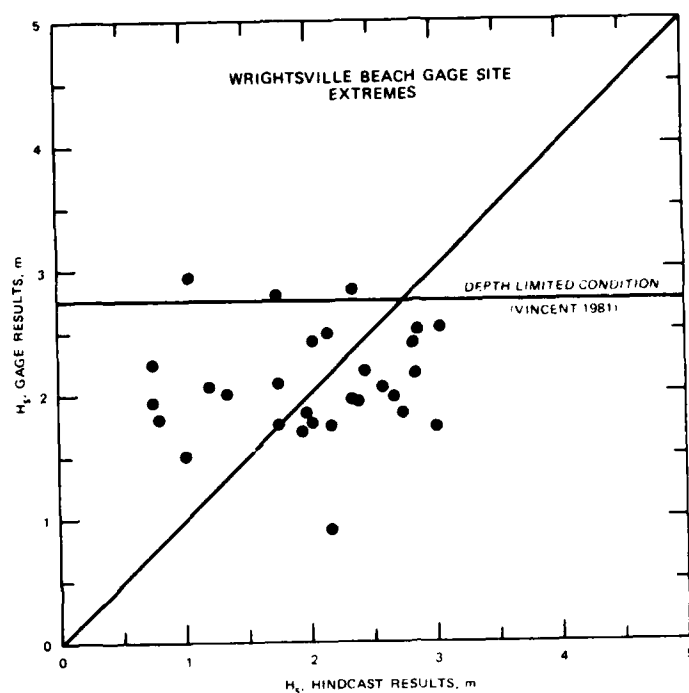


Figure 18. Cross plot of measured ( $h = 5.2$  m) and computed ( $h = 10$  m) maximum  $H_s$  conditions occurring in a specific event for Wrightsville Beach, North Carolina

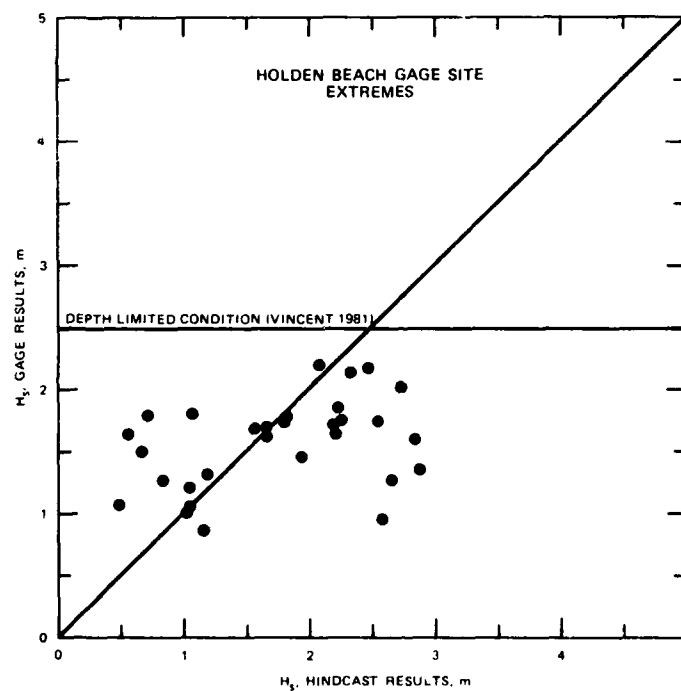


Figure 19. Cross plot of measured ( $h = 4.6$  m) and computed ( $h = 10$  m) maximum  $H_s$  conditions occurring in a specific event for Holden Beach, North Carolina

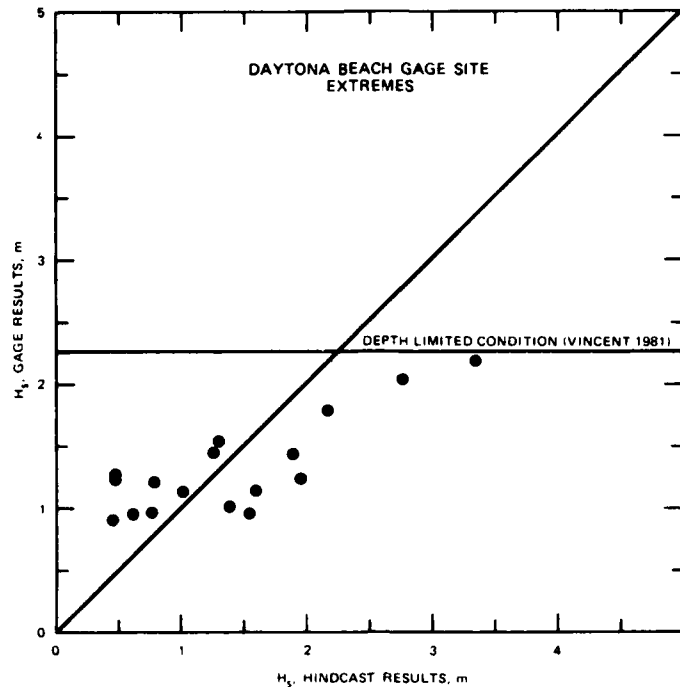


Figure 20. Cross plot of measured ( $h = 3.4$  m) and computed ( $h = 10$  m) maximum  $H_s$  conditions occurring in a specific event for Daytona Beach, Florida

straight shoreline segments. This coastline has numerous bays and off-shore islands which negate the straight and parallel bottom contours assumption. For this area, all Phase III shoreline station segments are aligned with the outermost offshore islands. Embayments, tidal inlets, and sounds are neglected whenever they exist within a given Phase III station section. In some instances, adjustments must be made for large offshore shoals (for example, Nantucket Shoal, Massachusetts, and Frying Pan Shoal, North Carolina). Also, wave conditions west of Cape Cod, Massachusetts, may only be a gross approximation of the actual wave conditions. Table 2 lists certain Phase III station locations (shown in Plates 1-6) along the Atlantic coast where "site-specific" modeling should be utilized to accompany the Phase III wave information.

69. The comparisons between gage and hindcast results demonstrated that the accuracy of the Phase III hindcasting technique is not lost while increasing computational efficiency. These comparisons have shown that the hindcast represents existing wave conditions (time-paired

and statistically) considering all variables associated with gaging operations. As in the case of the Phase I hindcast wave data (Corson and Resio 1981), the shallow-water (Phase III) wave data did not consistently overpredict nor underpredict the measured  $H_s$  conditions, although the hindcast  $T_p$  data showed a slight bias toward lower wave periods. The absolute cause of these differences cannot be defined; therefore a clear-cut adjustment to the hindcast  $T_p$  data cannot be made. The hindcast wave data presented in WIS Report 9 (Jensen 1983) should be used "as is" for ocean engineering projects.

## References

- Battjes, J. A. 1972. "Set-Up due to Irregular Waves," Report No. 72-2, Delft University of Technology, Department of Civil Engineering, Delft, The Netherlands.
- Corson, W. D., and Resio, D. T. 1981 (May). "Comparisons of Hindcast and Measured Deepwater Significant Wave Heights," WIS Report 3, U. S. Army Engineer Waterways Experiment Station, CE, Vicksburg, Miss.
- Goda, Y. 1974. "Estimation of Wave Statistics from Spectral Information," Proceedings, International Symposium on Ocean Wave Measurement and Analysis, American Society of Civil Engineers, Vol 1, pp 320-337.
- Hasselmann, K. et al. 1976. "A Parametric Wave Prediction Model," Journal of Physical Oceanography, Vol 6, pp 200-228.
- Hasselmann, K. et al. 1973. "Measurements of Wind-Wave Growth and Swell Decay During the Joint North Sea Wave Project JONSWAP," Dtsch, Hydrogr. Z., Vol 8, Supplement A8, No. 12.
- Heterich, K., and Hasselmann K. 1980. "A Similarity Relation for the Non-Linear Energy Transfers in a Finite-Depth Gravity-Wave Spectrum," Journal of Fluid Mechanics, Vol 97, Part 1, pp 215-224.
- Hsiao, Shu-Chi, Vincent. 1978. On the Transformation Mechanisms and the Prediction of Finite-Depth Water Waves, Ph. D. Dissertation, University of Florida, Gainesville, Fla.
- Iwata, Koichiro. 1980. "Wave Spectrum Changes due to Shoaling and Breaking. I - Minus - Three - Power - Law on Frequency Spectrum," Technical Report, Osaka University, Vol 30, No. 1517-1550, pp 269-278.
- Jensen, R. E. 1983 (Jan). "Atlantic Coast Hindcast, Shallow-Water Significant Wave Information," WIS Report 9, U. S. Army Engineer Waterways Experiment Station, CE, Vicksburg, Miss.
- Kitaigorodskii, S. A. 1962. "Application of the Theory of Similarity to the Analysis of Wind-Generated Wave Motion as a Stochastic Process," Bull. Acad. Sci. USSR Ser. Geophys., No. 1, Vol. 1, pp. 105-117.
- Kitaigorodskii, S. A., Krasitskii, V. P., and Zaslavskii, M. M. 1975. "On Phillips' Theory of Equilibrium Range in the Spectra of Wind-Generated Gravity Waves," Journal of Physical Oceanography, Vol 5, pp 410-420.
- Ou, Shan-Hwei. 1980. "The Equilibrium Range in the Frequency Spectra of the Wind Generated Gravity Waves," Proceedings, 4th Conference on Ocean Engineering in the Republic of China.
- Pierson, W. J., and Moskowitz, L. 1964. "A Proposed Spectral Form for Fully Developed Wind Seas Based on the Similarity Theory of S. A. Kitaigorodskii," Journal of Geophysical Research, Vol 60, pp 5181-5190.
- Resio, D. T. 1978. "Estimation of Longshore Drift Rates from Numerical Models," Coastal Zone '78, American Society of Civil Engineers, Vol III, pp 2289-2307.

Resio, D. T. 1981. "The Estimation of Wind-Wave Generation in a Discrete Spectral Model," Journal of Physical Oceanography, Vol 11, No. 4, pp 510-525.

Sell, W., and Hasselmann, K. 1972. "Computations of Non-Linear Energy Transfer for JONSWAP and Empirical Wind Wave Spectrum," Institute of Geophysics, University of Hamburg, Hamburg, Germany.

Shemdin, O. H., et al. 1980. "Mechanisms of Wave Transformation in Finite-Depth Water," Journal of Geophysical Research, Vol 85, No. C9, pp 5012-5018.

Skovgaard, O., Jonssen, I. G., and Bertelsen, J. A. 1975. "Computation of Wave Heights due to Refraction and Friction," Journal of the Waterways Harbors and Coastal Engineering Division, American Society of Civil Engineers, Vol 101, No. WW1, pp 15-32.

Thompson, E. F. 1977. "Wave Climate at Selected Locations Along U. S. Coasts," Technical Report No. 77-1, U. S. Army Coastal Engineering Research Center, Fort Belvoir, Va.

Thornton, E. B. 1977. "Rederivation of the Saturation Range in a Frequency Spectrum of Wind-Generated Gravity Waves," Journal of Physical Oceanography, Vol 7, pp 137-140.

Vincent, C. L. 1981. "A Method for Estimating Depth-Limited Wave Energy," CETA No. 81-16, U. S. Army Coastal Engineering Research Center, CE, Fort Belvoir, Va.

\_\_\_\_\_. 1982 (May). "Shallow Water Wave Modeling," 1st International Conference on Meteorology and Air-Sea Interaction in the Coastal Zone, The Hague.

Table 1  
Physical Parameters Associated with Gage Sites

Gage Site Name	Location	Data Set Dates	Water Depth m	Gage Type
Nauset, Mass.	41.8°N, 69.93°W	1974-1975	10.67	Pressure (1/74-12/75)
Southampton, N. Y.	40.85°N, 72.42°W	1973-1975	9.76	Pressure (N/A)
Nags Head N. C.	35.92°N, 75.60°W	1968-1975	5.18	Step-resistance (19/63-10/72) Continuous wire (11/72-12/75)
Wrightsville Beach, N. C.	34.22°N, 77.78°W	1971-1975	5.18	Step-resistance (3/70-12/74) Continuous wire (1/75-12/75)
Holden Beach, N. C.	33.92°N, 78.30°W	1971-1975	4.57	Continuous wire (2/71-12/75)
Daytona Beach Fla.	29.15°N, 80.97°W	1969-1971	3.35	Pressure (11/64-12/75)

Table 2

## Limiting Approximations Associated with Certain Phase III Station Wave Data

Station Number	Description	Approximation Employed
1-15*	Straight shoreline segment assumption may not be appropriate due to complex shorelines	Assumed shoreline at outer-most islands, neglected all bays
24	Lack of detail in the Phase II modeling restricted resolution of Phase III data	Phase III station neglects Boston Harbor Bay
27	Lack of detail in the Phase II modeling restricted resolution of Phase III data	Phase III station neglects Cape Cod Bay
33	Transformation mechanisms are undeterminable over shoals, require site-specific modeling	Phase III station neglects Nantucket Shoal
53	Wave and current interactions are not qualified	Phase III station neglects New York Bay and all current interactions
64	Wave and current interactions are not qualified	Phase III station neglects influences from Delaware Bay
76	Wave and current interactions are not qualified	Phase III station neglects influence from Chesapeake Bay
87-88	Transformation mechanisms are undeterminable over shoals, require site-specific modeling	Phase III stations neglect shoals around Cape Hatteras
94-95	Transformation mechanisms are undeterminable over shoals, require site-specific modeling	Phase III stations neglect Cape Lookout Shoals
104-106	Transformation mechanisms are undeterminable over shoals, require site-specific modeling	Phase III stations neglect Frying Pan Shoals

\* See Plates 1-6 for geographical location of the Phase III stations.

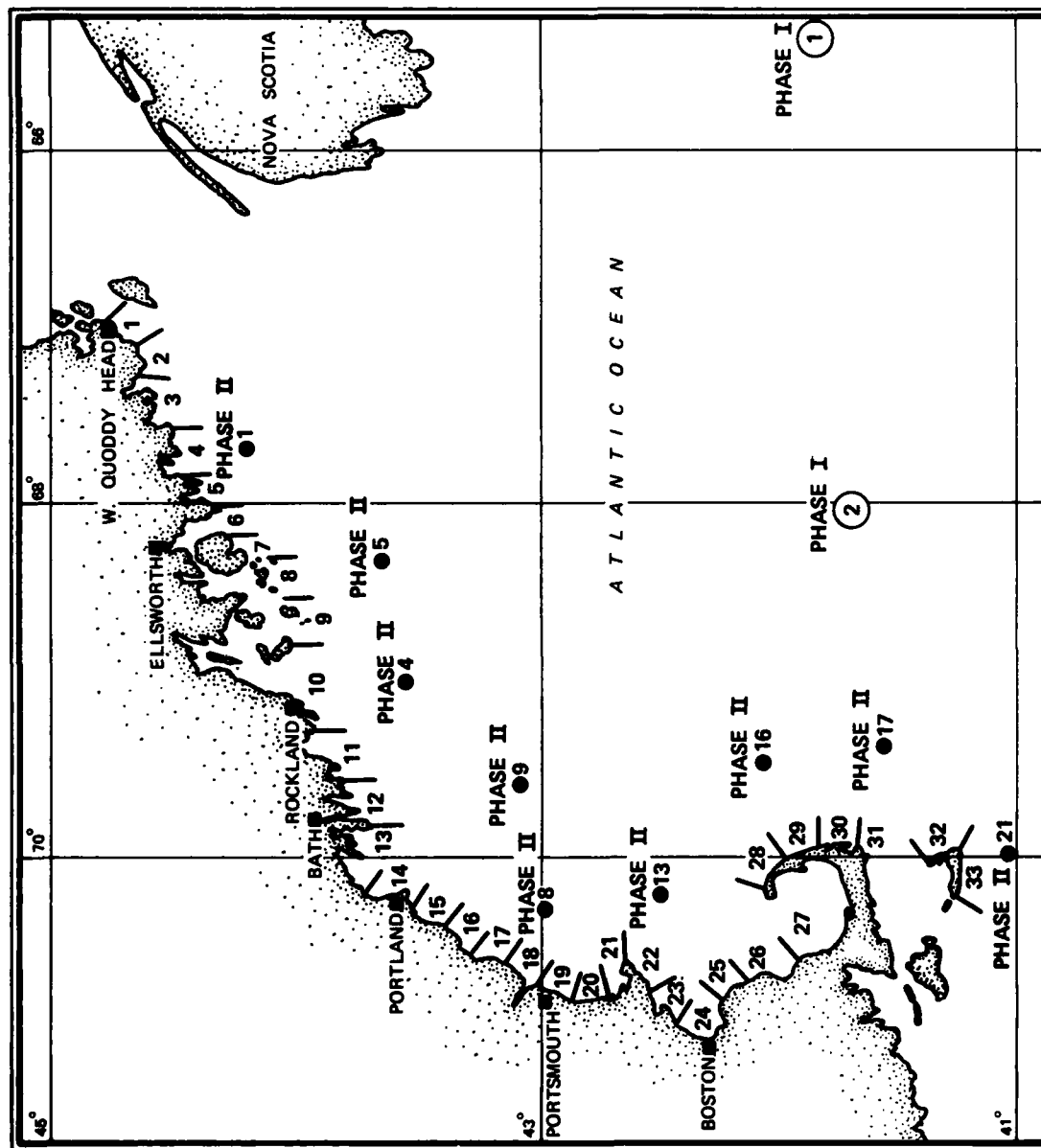


Plate 1. Locations of Phase III stations for shallow-water wave information along the Atlantic coast, Region 1



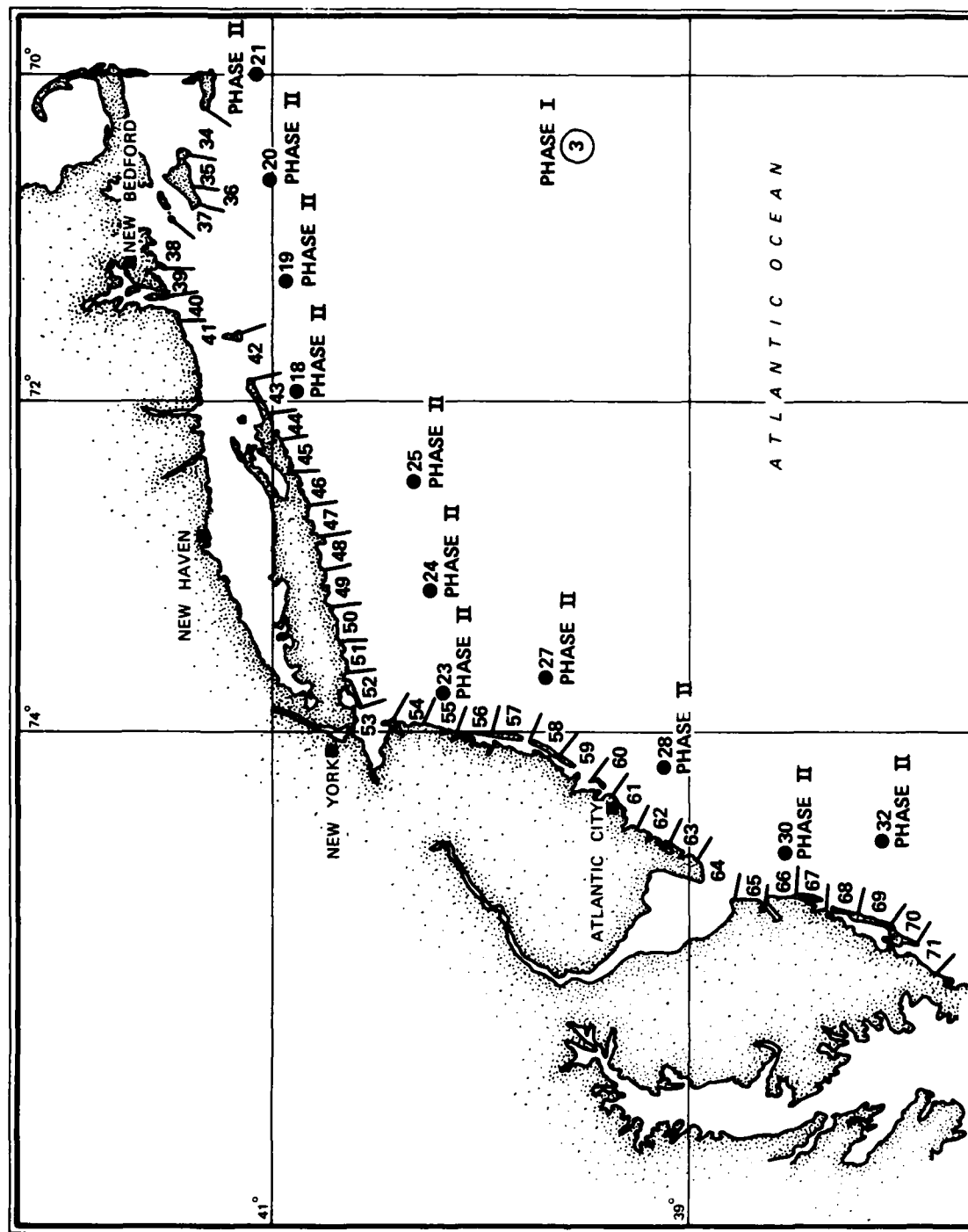


Plate 2. Locations of Phase III stations for shallow-water wave information along the Atlantic coast, Region 2

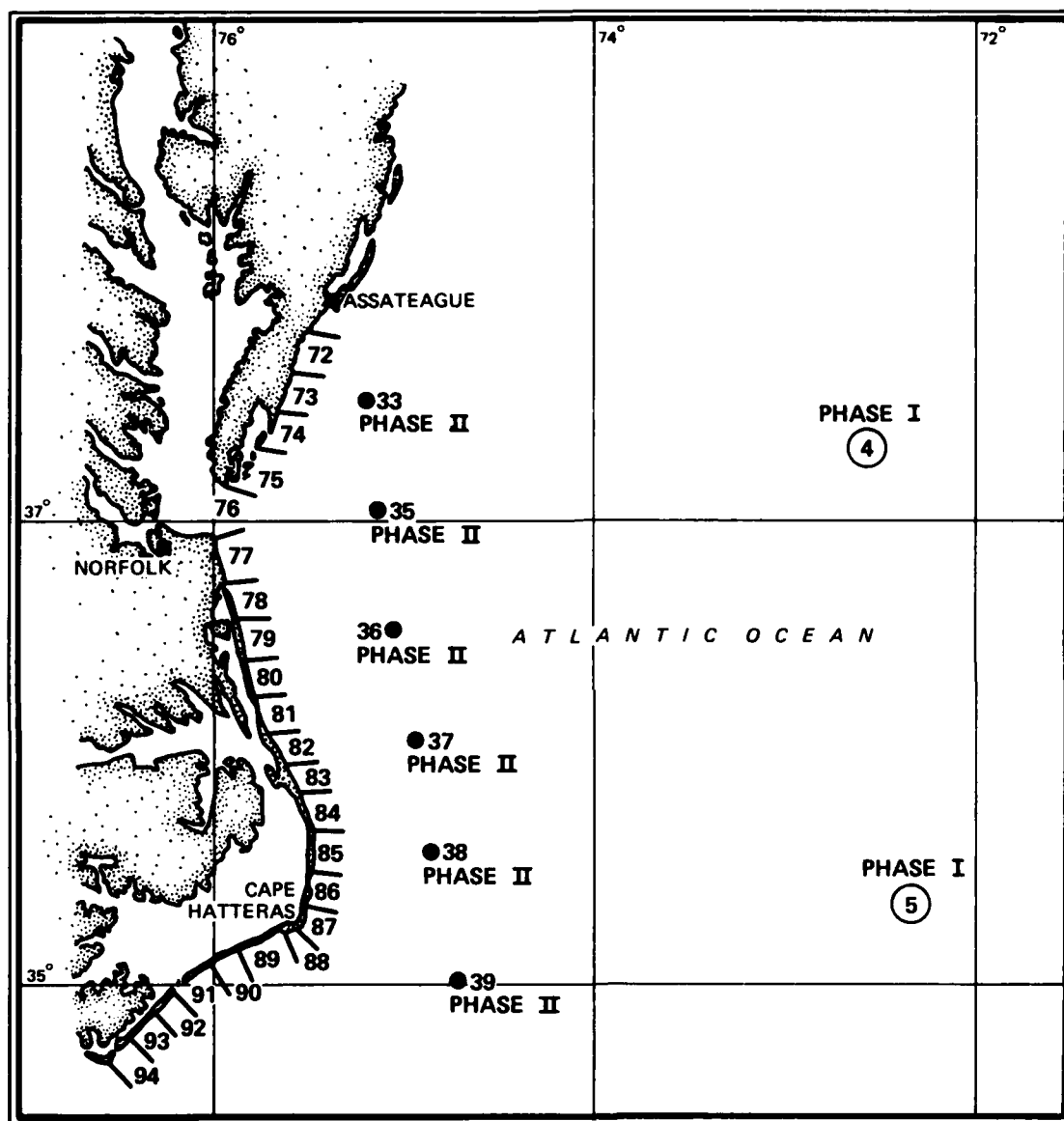


Plate 3. Locations of Phase III stations for shallow-wave wave information along the Atlantic coast, Region 3

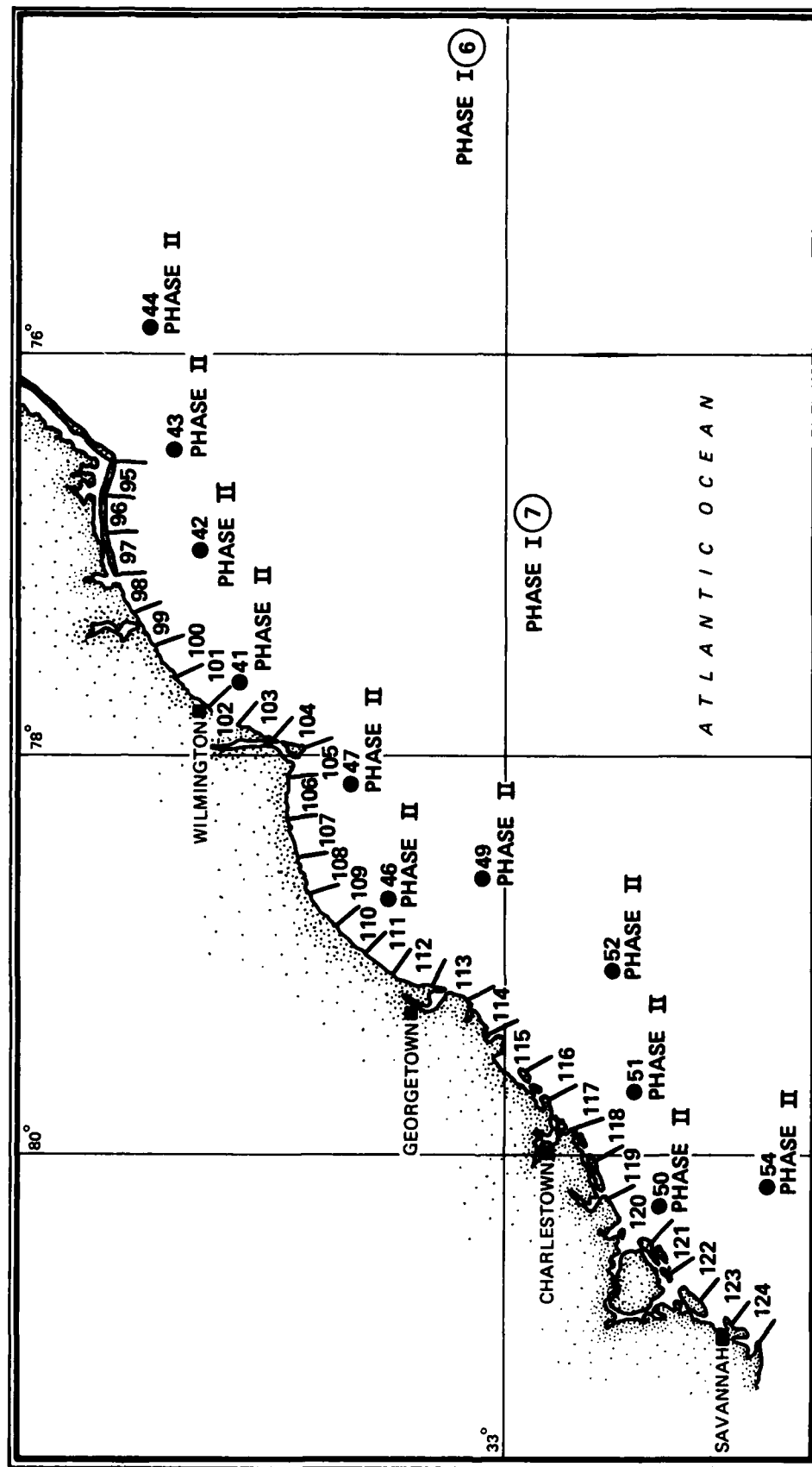


Plate 4. Locations of Phase III stations for shallow-water wave information along the Atlantic coast, Region 4

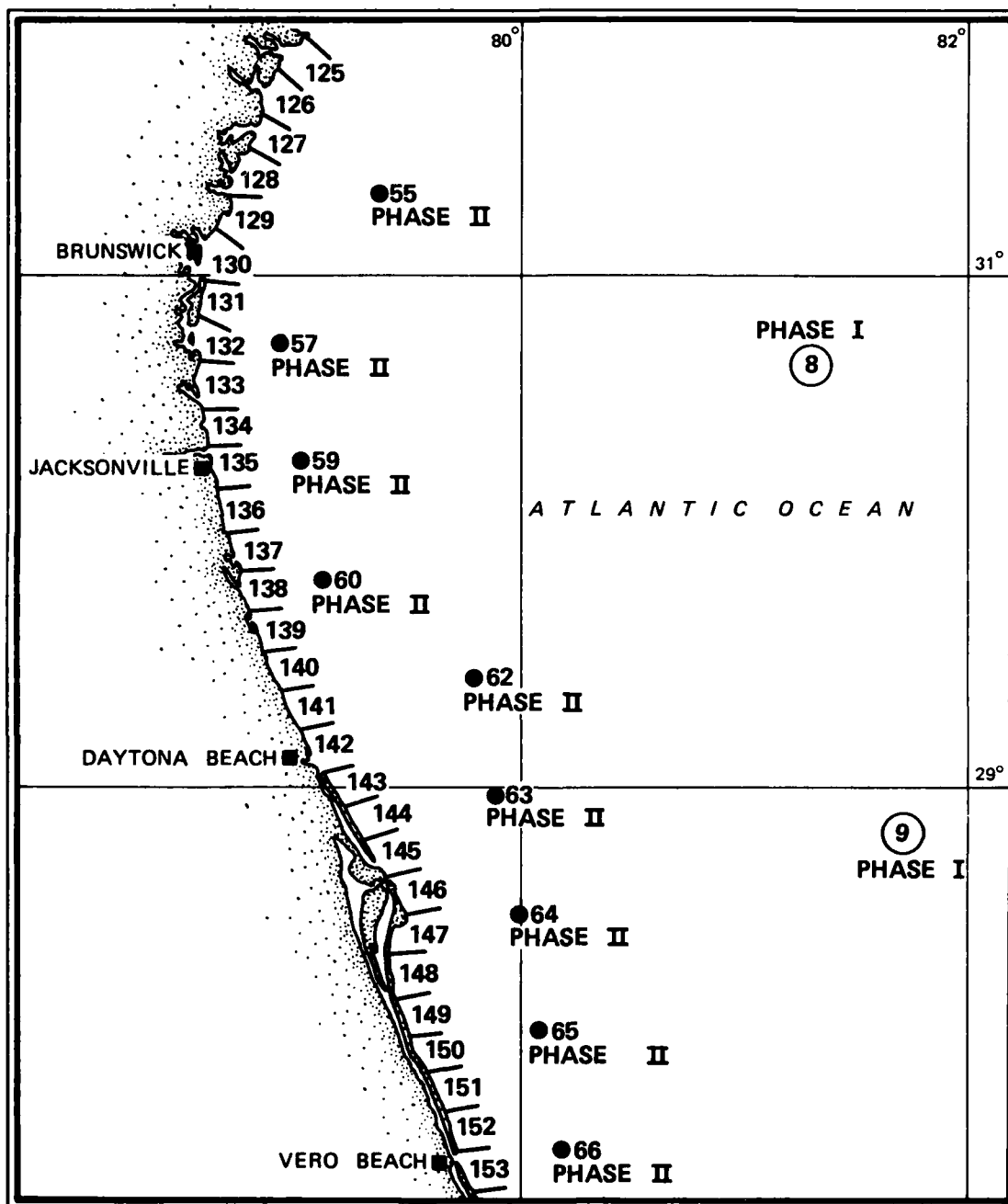


Plate 5. Locations of Phase III stations for shallow-water wave information along the Atlantic coast, Region 5

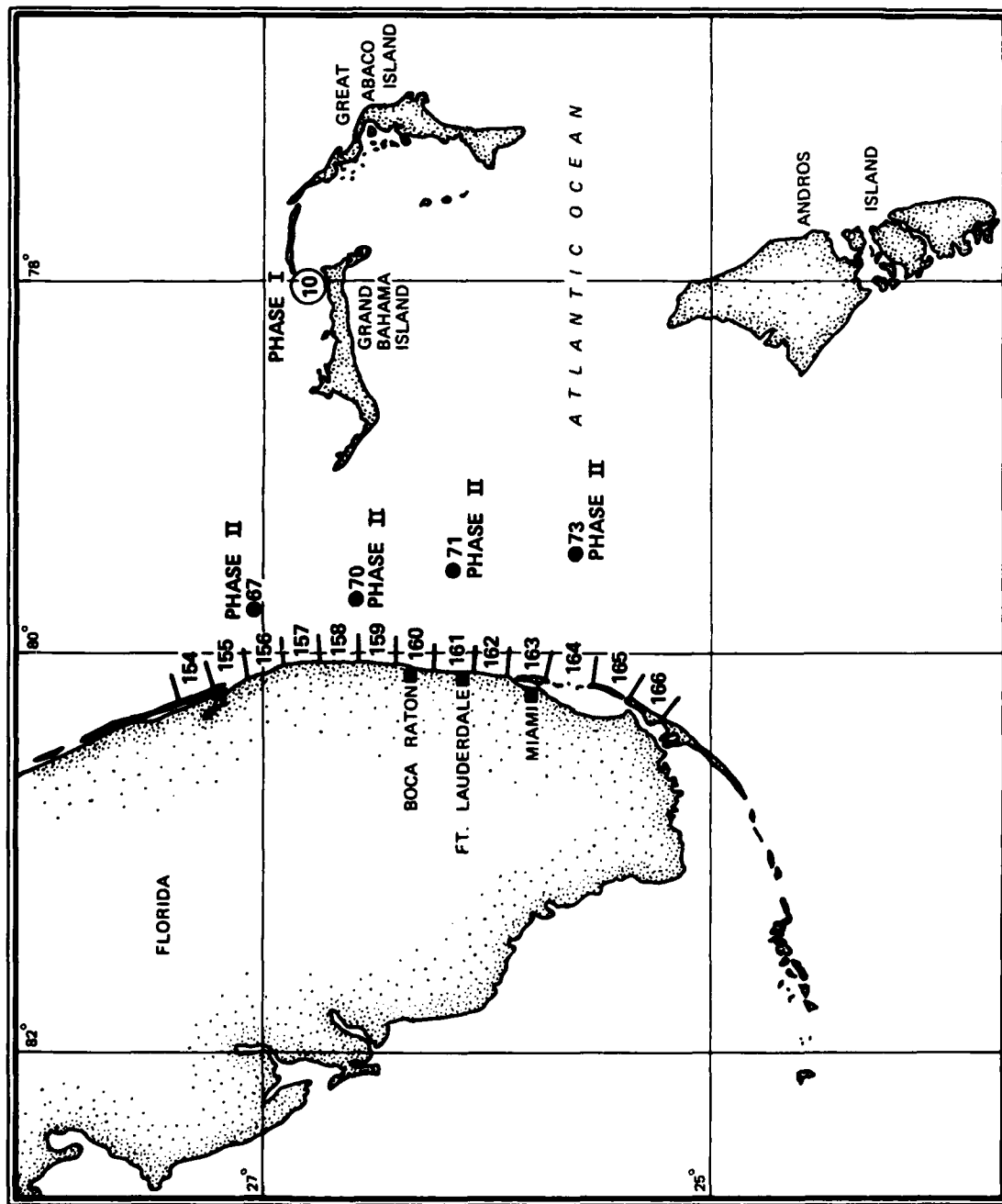


Plate 6. Locations of Phase III stations for shallow-water wave information along the Atlantic coast, Region 6

Appendix A: Mathematical Treatment of the Transformation of  
Probabilities from One Coordinate System into Another

1. Given an operator such that one set of parameters  $W_1, \dots, W_n$  can be uniquely mapped into another coordinate system  $W'_1, \dots, W'_n$ ,

$$W'_i = \phi_i(W_1, \dots, W_n) \quad (A1)$$

$$W_i = \phi_i^{-1}(W'_1, \dots, W'_n) \quad (A2)$$

then a probability density function in  $\underline{W}$  can be transformed into a probability density function in  $\underline{W}'$ ,

$$\begin{aligned} & p(W'_1, \dots, W'_n) \\ &= p\left[\phi_1(W_1, \dots, W_n), \dots, \phi_n(W_1, \dots, W_n)\right] |J| \end{aligned} \quad (A3)$$

where  $J$  is the Jacobian of the transformation

$$J = \begin{vmatrix} \frac{\partial W'_1}{\partial W_1} & \frac{\partial W'_2}{\partial W_1} & \dots & \frac{\partial W'_n}{\partial W_1} \\ \frac{\partial W'_1}{\partial W_2} & \frac{\partial W'_2}{\partial W_2} & \dots & \frac{\partial W'_n}{\partial W_2} \\ \dots & \dots & \dots & \dots \\ \frac{\partial W'_1}{\partial W_n} & \frac{\partial W'_2}{\partial W_n} & \dots & \frac{\partial W'_n}{\partial W_n} \end{vmatrix}$$

For an increment of probability, the relationship between probabilities in the different parameter spaces can be written as

$$\begin{aligned}
& p(W'_1, \dots, W'_n)(\Delta W'_1, \dots, \Delta W'_n) \\
&= p[\phi_1(W_1, \dots, W_n), \dots, \phi_n(W_1, \dots, W_n)] \\
&\quad \times [\Delta \phi_1(W_1, \dots, W_n), \dots, \Delta \phi_n(W_1, \dots, W_n)] \quad . \quad (A4)
\end{aligned}$$

Or, in terms of mapping a continuous function from  $\underline{W}$  into  $\underline{W}'$  would yield

$$\begin{aligned}
& \int_R \dots \int p(W'_1, \dots, W'_n) dW'_1 \dots dW'_n \\
&= \int_S \dots \int p(W_1, \dots, W_n) dW_1 \dots dW_n \quad (A5)
\end{aligned}$$

where the limits of region  $R$  are defined by applying the operator  $\phi$  to the limits of  $S$ . Vice versa, the limits of  $S$  can be obtained by applying the inverse operator  $\phi^{-1}$  to  $R$ .

2. Numerical estimation techniques for probabilities generally deal with a discretized representation of the probability density function; consequently, one needs to transform Equation 5 in terms of a discretized approximation. Given  $\underline{r}$  as an incremental index to the location of a discrete category in  $\underline{W}$ , probability increments of  $\underline{r}$  can then be mapped into probability increments in  $\underline{r}'$  in an analogous manner to Equation 5. Letting  $p'$  denote the discretized probability density function in  $\underline{r}'$  space,

$$p'(r'_1, \dots, r'_n) = \sum_{r_i=j_i}^{k_i} \dots \sum_{r_n=j_n}^{k_n} p(r_1, \dots, r_n) \quad (A6)$$

where  $(j_i, k_i), \dots, (j_n, k_n)$  are the discretized limits in region  $S$  in  $\underline{W}$  corresponding to a given incremented region  $R$  in  $\underline{W}'$ .

3. Thus when a small set of parameters is sufficient to categorize a probability function for practical purposes, it is feasible to approach the transformation of probabilities from one such parameter

space into a related parameter space by storing indices in one coordinate system as a function of indices in the related coordinate system. This method is particularly advantageous when the form of  $\phi$  is not a simple analytic function of all parameters. In such a case, the evaluation of the Jacobian must be done numerically, which can be exceedingly tedious. Such complex, nonlinear forms for  $\phi$  are typical in nearshore wave transformation processes. An approximation of the following form can be used for such transformations.

4. First, determine  $r'_1 = (r_1, \dots, r_n)$ . This represents a mapping of the central point of the discretized category  $r_1, \dots, r_n$  into a discretized category  $r'_1 \dots r'_n$ . For each discretized category in parameter space  $\underline{r}$  there will be a unique corresponding discretized category in  $\underline{r}'$ . In this manner, an approximation for a probability density function in  $\underline{r}'$  can be formed from a probability density function in  $\underline{r}$ .

$$p(r'_1, \dots, r'_n) = \sum_{r_1} \dots \sum_{r_n} p(r_1, \dots, r_n) \delta[\phi(\underline{r}) - r'] \quad (A7)$$

where the delta function  $\delta[\phi(\underline{r}) - r']$  ensures that  $\dots dp$  is conserved in the mapping. Since Equation 7 represents the mapping of discrete probability increments rather than probability densities, some bias will be generated by this operation; however, if the incrementization is small the bias should be minimal. Also, additional accuracy can be obtained by modifications to Equation 7 which consider a gradient in  $p$  across an increment in  $\underline{r}'$ . For the present, Equation 7 will be used as written to obtain the approximation to  $p(\underline{r}')$ , with the exception that in practice the delta function behavior is obtained numerically by stepping through indices  $\underline{r}$  (only once) into its appropriate category in  $\underline{r}'$ .



## Appendix B: Comparison of Spectral and Monochromatic Representation for Refraction and Shoaling

1. Since most engineers are more familiar with the monochromatic representations for refraction and shoaling, a comparison with the spectral representations is included here, along with a comparison of the differences predicted by the two methods. The traditional conservation of energy flux in monochromatic wave is written as

$$(c_g E b) = \left( c_g E b \right)_o \quad (B1)$$

where  $c_g$  is the group velocity,  $E$  is wave energy,  $b$  is the width between two adjacent wave rays, and the subscript  $o$  refers to initial conditions (deep water). Figure B1 shows two wave rays coming into a coast. The spacing between the rays can be shown to be equal to a projection of an orthogonal onto a plane parallel to the depth contours; hence the ratio of  $b$  to  $b_o$  can be defined in terms of the cosines of the angles  $\theta$  and  $\theta_o$ .

$$\frac{b}{b_o} = \frac{\cos \theta}{\cos \theta_o} \quad (B2)$$

where  $\theta_o$  and  $\theta$  are the initial angle and subsequent angles along the wave ray, respectively. This ratio  $b_o/b$  is commonly referred to as the refraction coefficient and the ratio  $c_{g_o}/c_g$ , the shoaling coefficient. From Equation B1 and B2, the energy along the ray can be written as

$$E = \left( \frac{\cos \theta_o}{\cos \theta} \right) \left( \frac{c_{g_o}}{c_g} \right) E_o \quad (B3)$$

2. If we now examine a narrow spectrum approaching in the limit a delta function in angle and frequency, Equation 12 yields

$$E = \int_0^{\infty} \int_0^{2\pi} E_2(f, \theta) \frac{(c c_g)_o}{(c c_g)} \left| \frac{\partial \theta}{\partial \theta_o} \right| d\theta_o df_o \quad (B4)$$

where  $E_2(f, \theta)$  is the initial energy distribution given by

$$E_2(f, \theta) = E_o \delta(\theta - \theta') \delta(f - f')$$

where  $\theta'$  is the central angle of the angular distribution and  $f'$  is the frequency of the spectral peak. Integrating over both delta functions gives

$$E = E_o \frac{(c c_g)_o}{(c c_g)} \left| \frac{\partial \theta}{\partial \theta_o} \right| \quad (B5)$$

From Snell's law we have:

$$\sin \theta = \frac{c}{c_o} \sin \theta_o \quad (B6)$$

Differentiating both sides with respect to  $\theta$  gives

$$\cos \theta = \frac{c}{c_o} \cos \theta \left| \frac{\partial \theta}{\partial \theta_o} \right| \quad (B7)$$

which when rearranged provides an evaluation for the partial derivative in Equation B5.

$$\left| \frac{\partial \theta}{\partial \theta_o} \right| = \frac{c}{c_o} \frac{\cos \theta_o}{\cos \theta} \quad (B8)$$

Substituting this into Equation B5 gives

$$E = E_o \frac{\cos \theta_o}{\cos \theta} \frac{c_g}{c} \quad (B9)$$

which is identical with Equation B3, as it should be for this case.

Appendix C: Plots of  $H_s$  and  $T_p$  Versus Time

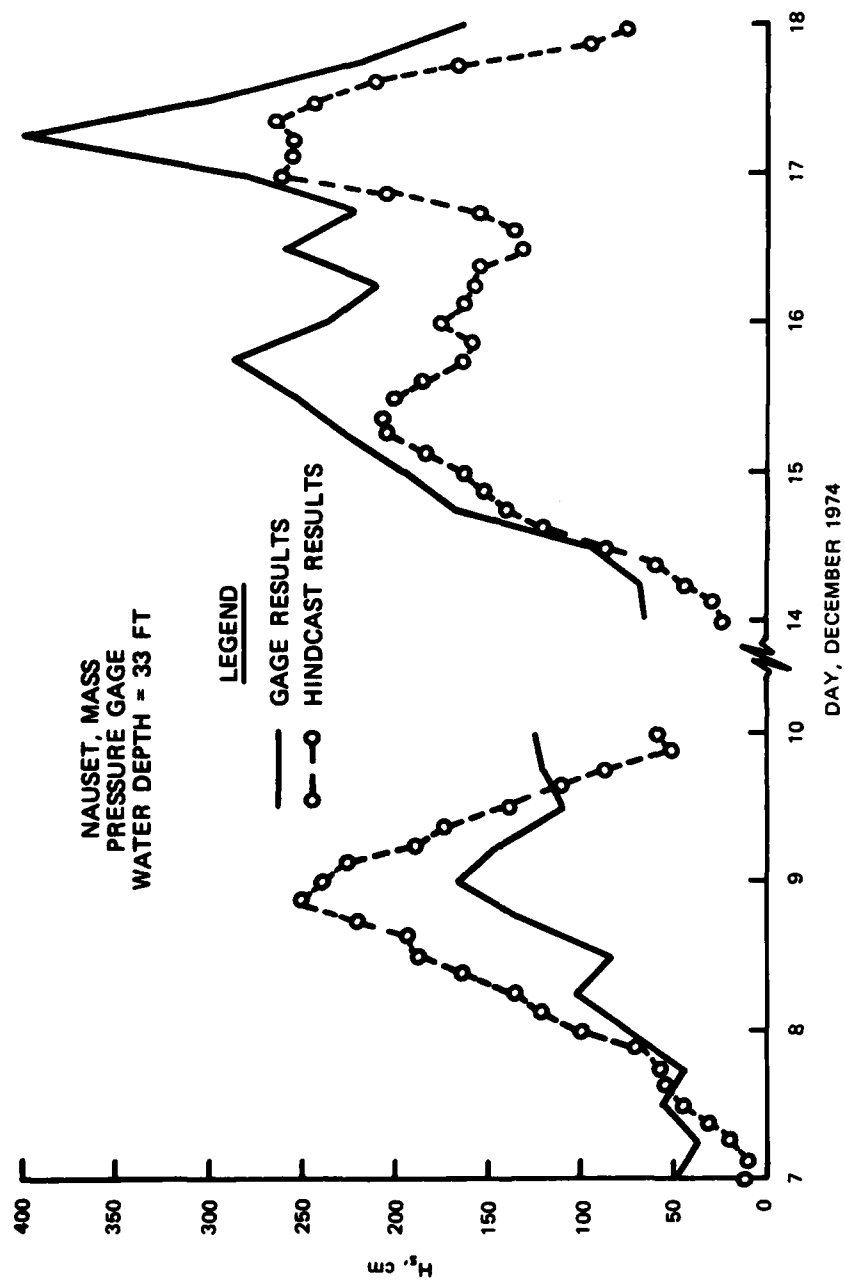


Figure C1. Plot of  $H_s$  versus time for a period in December 1974 for Nauset, Mass.

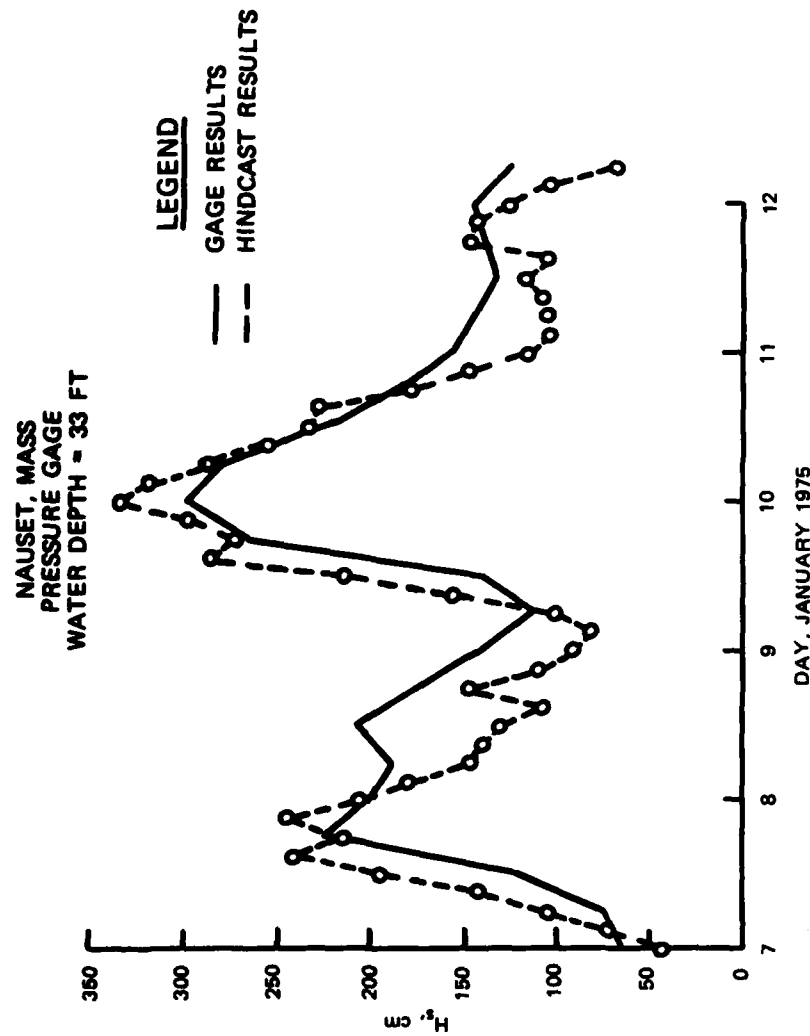


Figure C2. Plot of  $H_s$  versus time for a period in January 1975 for Nauset, Mass.

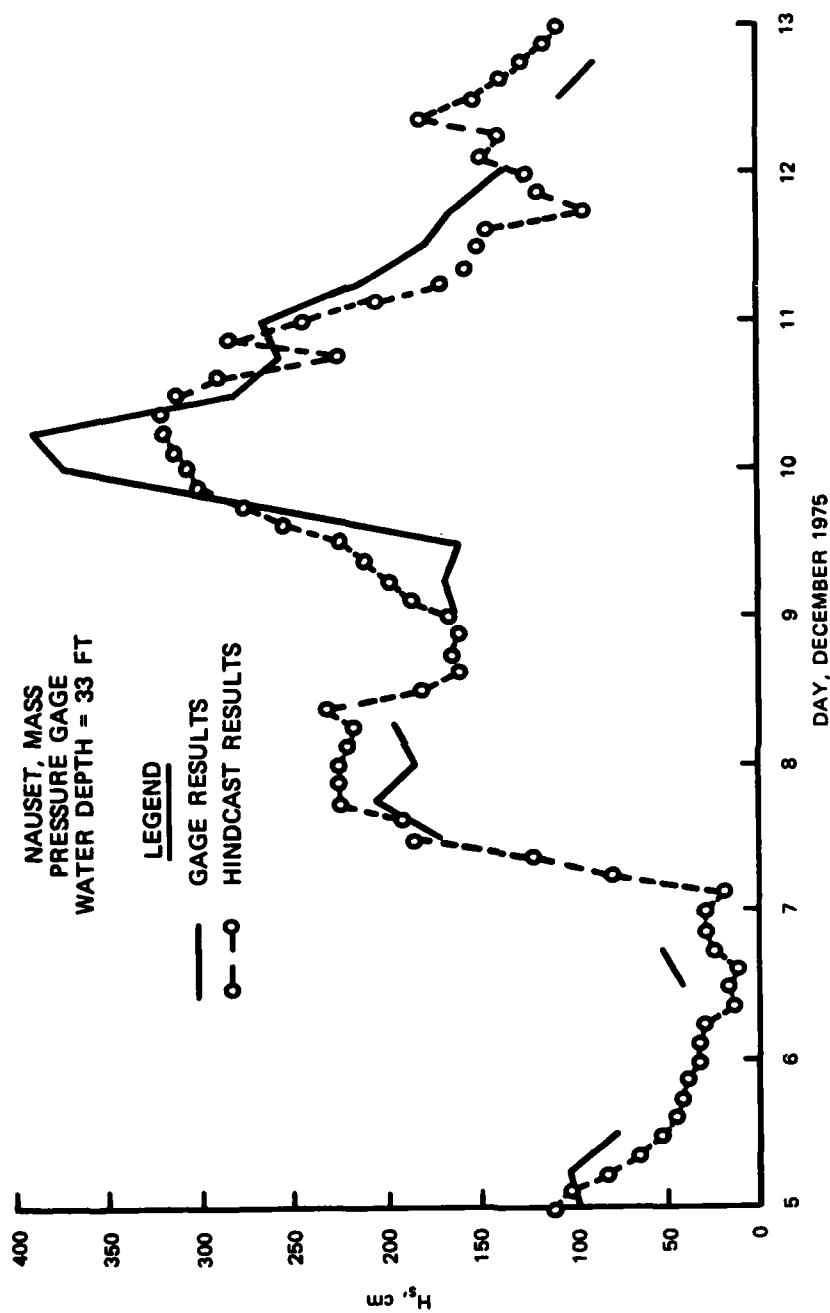


Figure C3. Plot of  $H_s$  versus time for a period in December 1975 for Nauset, Mass.

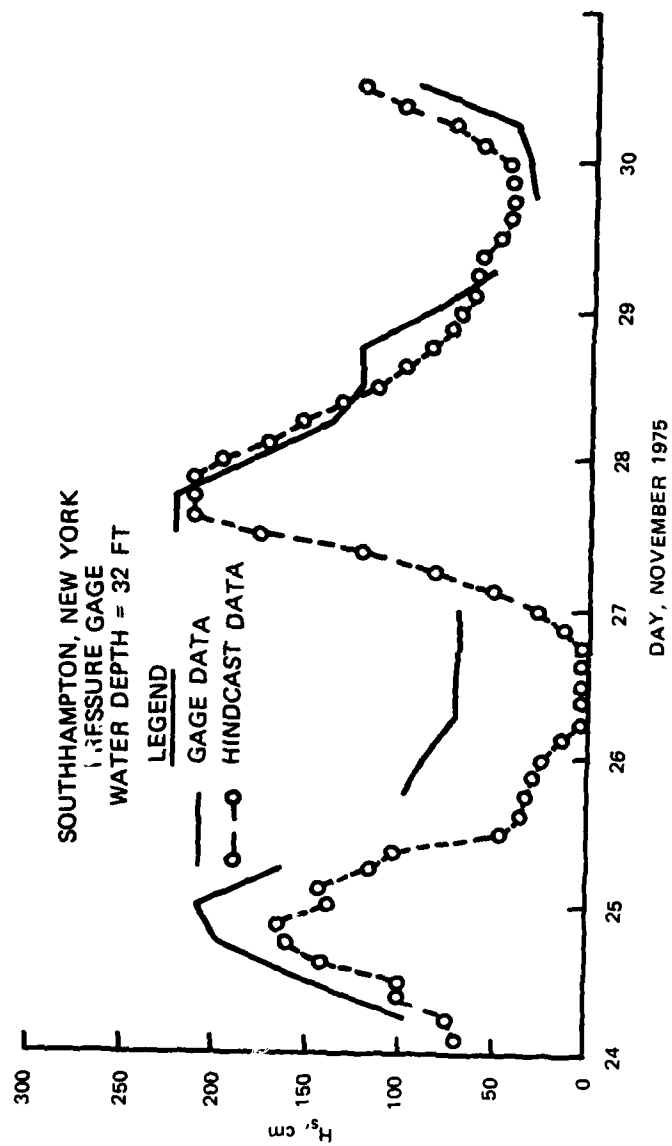


Figure C4. Plot of  $H_s$  versus time for a period in November 1975 for Southampton, New York

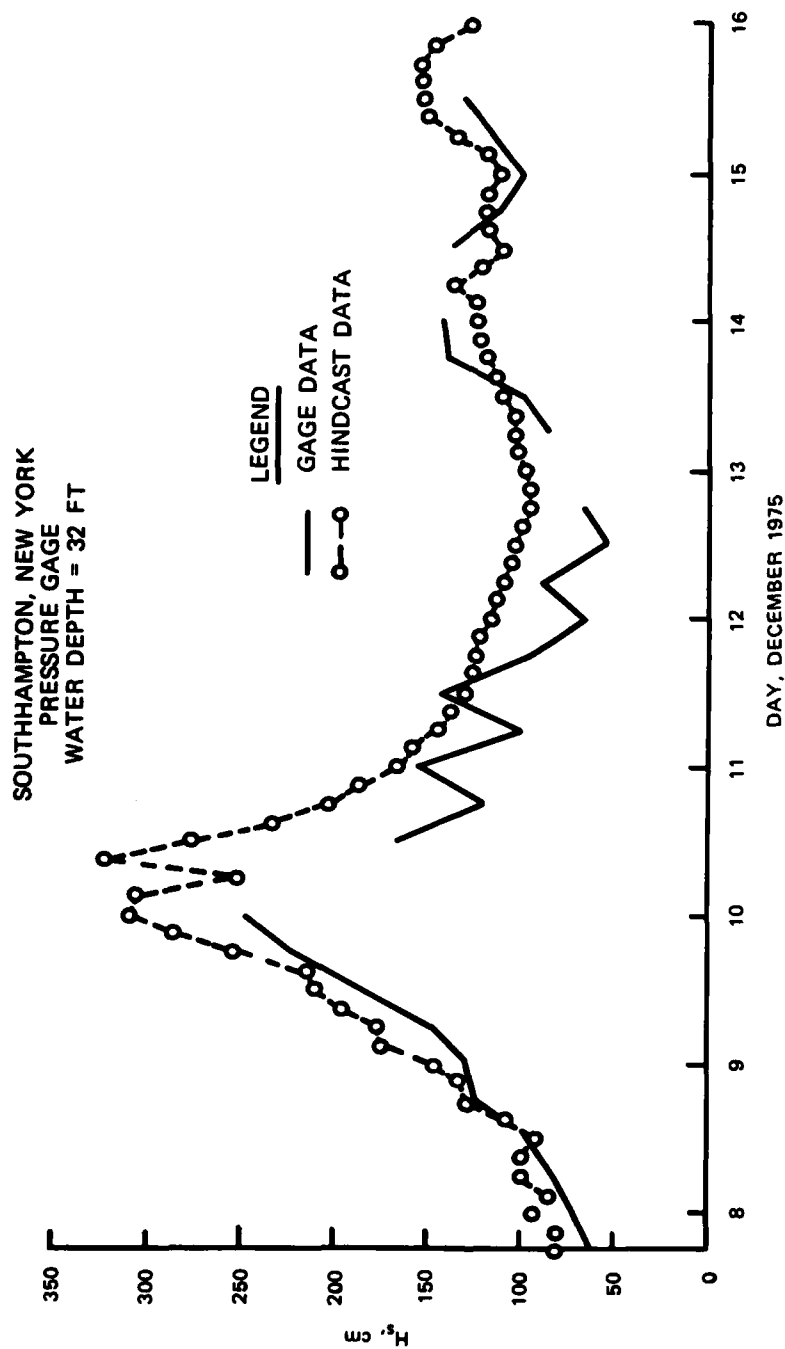


Figure C5. Plot of  $H_s$  versus time for a period in December 1975 for Southampton, New York



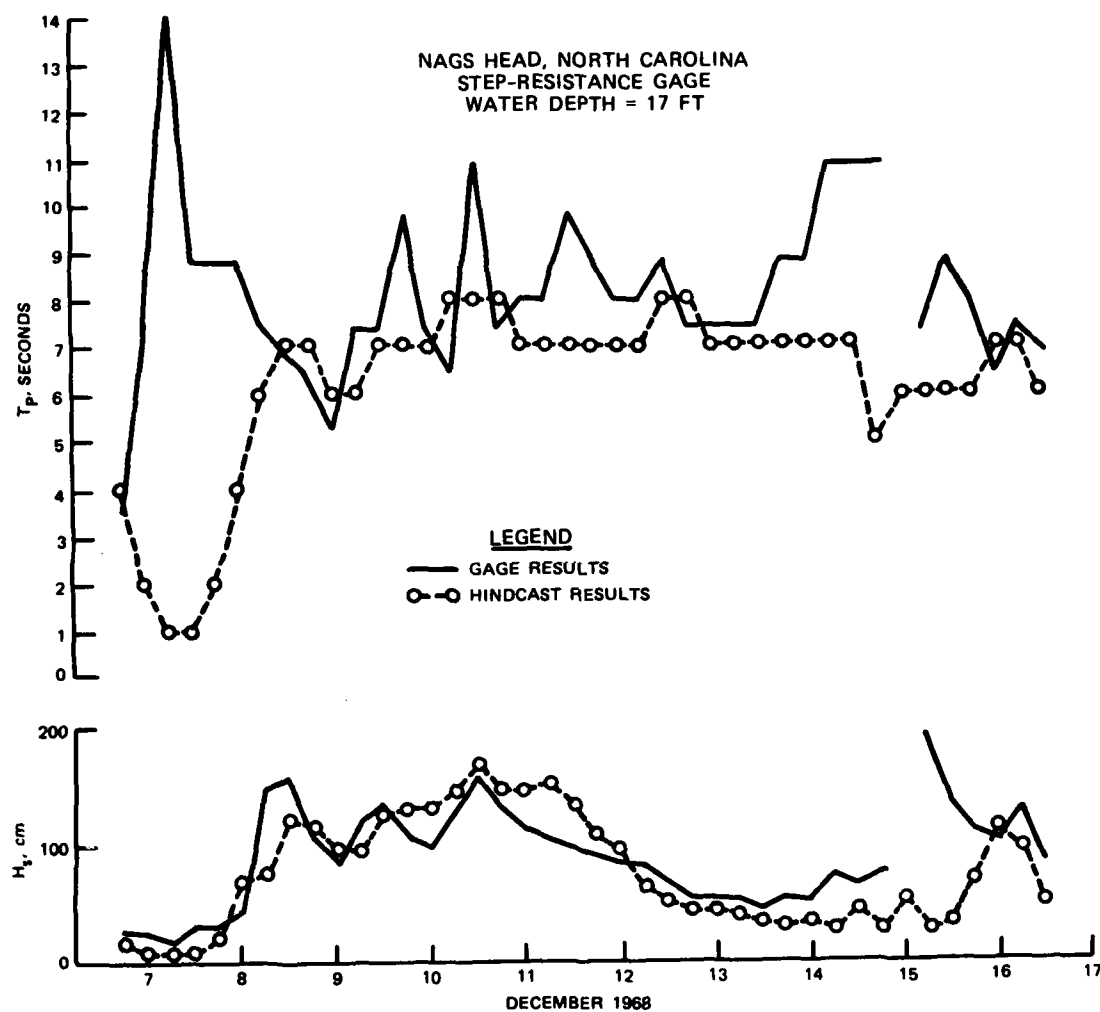


Figure C6. Plots of  $H_s$  and  $T_p$  versus time for a period in December 1968 for Nags Head, North Carolina

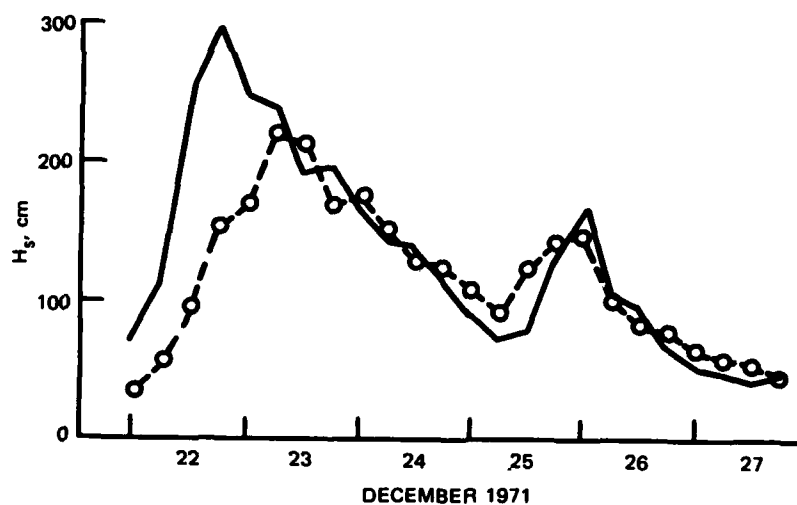
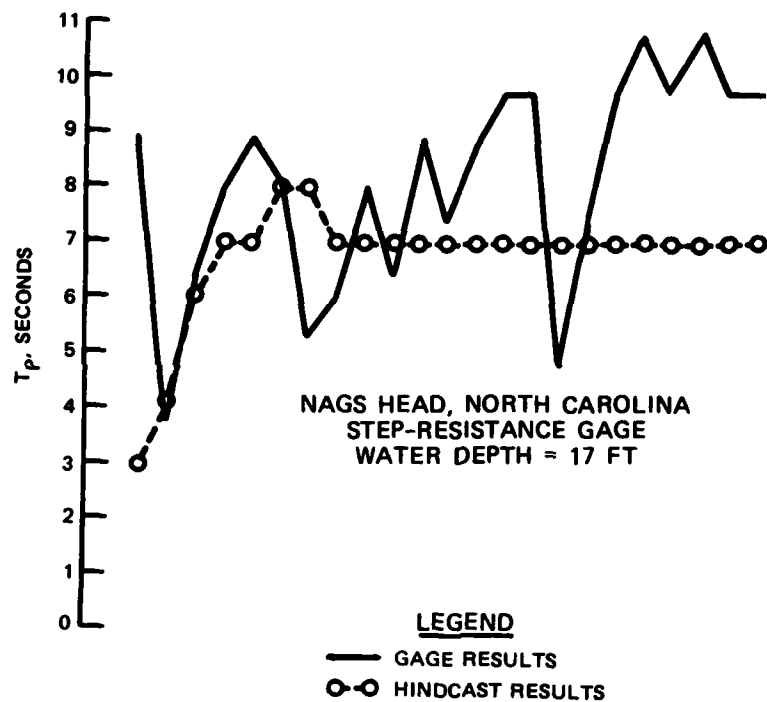


Figure C7. Plots of  $H_s$  and  $T_p$  versus time for a period in December 1971 for Nags Head, North Carolina

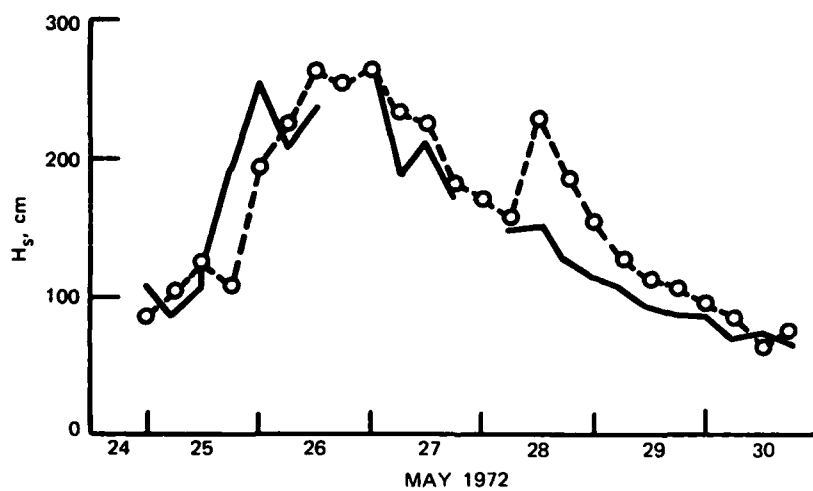
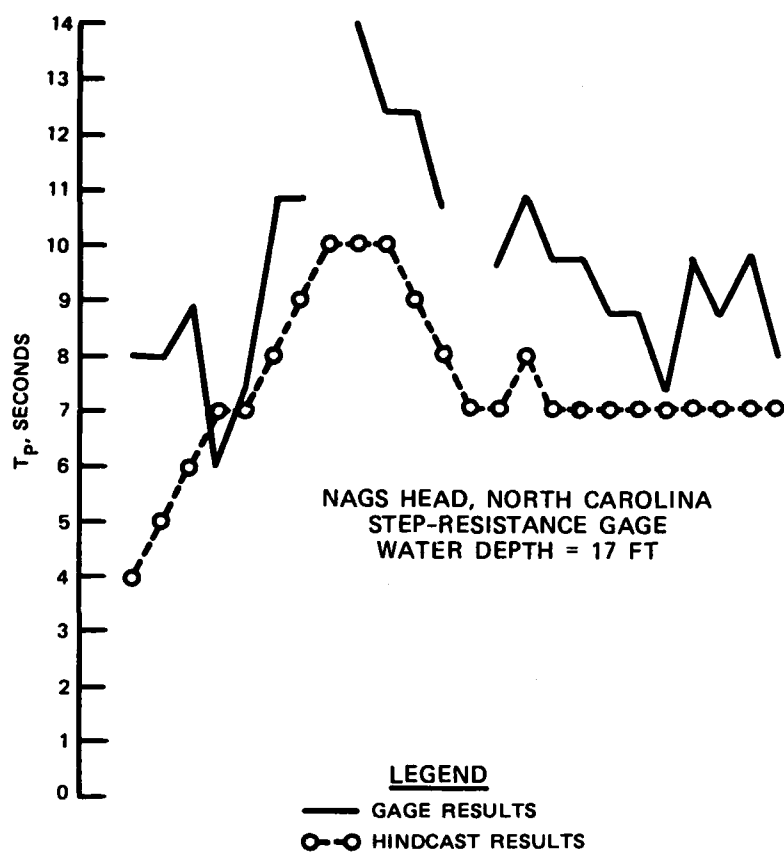


Figure C8. Plots of  $H_s$  and  $T_p$  versus time for a period in May 1972 for Nags Head, North Carolina

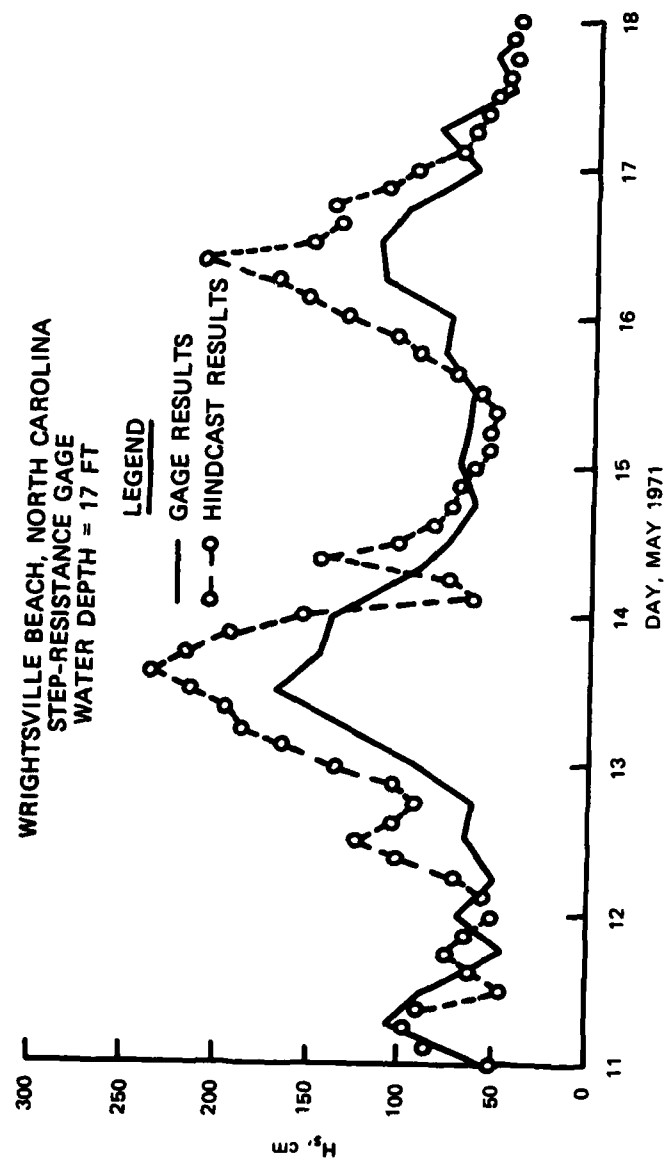


Figure C9. Plots of  $H_s$  versus time for a period in May 1971 for  
Wrightsville Beach, North Carolina

WRIGHTSVILLE BEACH, NORTH CAROLINA  
STEP-RESISTANCE GAGE  
WATER DEPTH = 17 FT

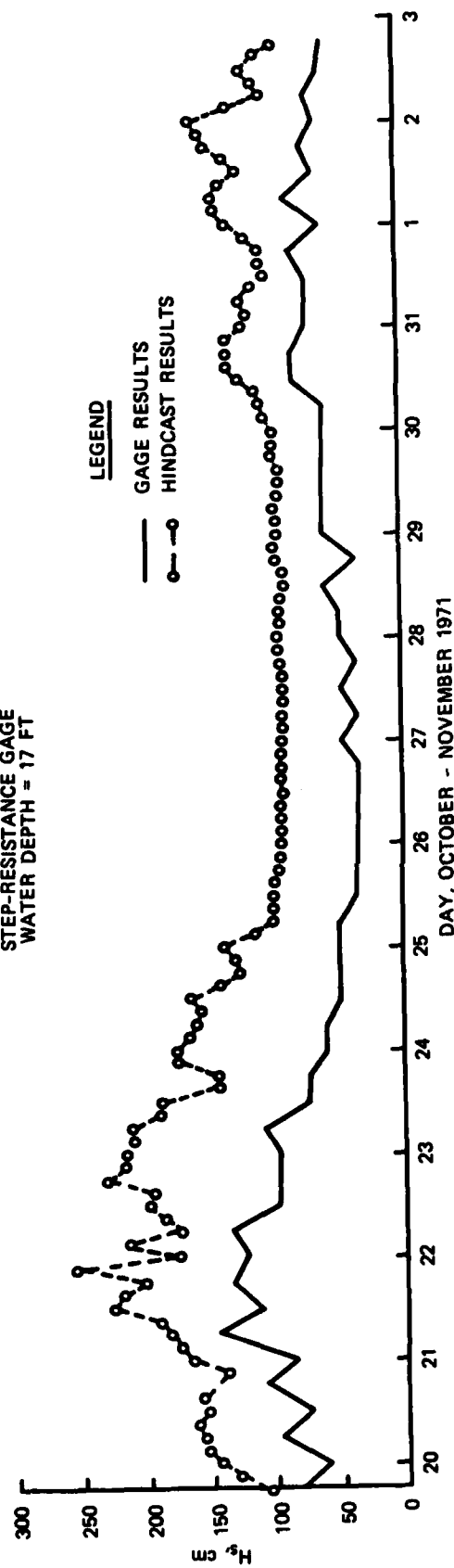


Figure C10. Plots of  $H_s$  versus time for a period in October-November 1971 for Wrightsville Beach, North Carolina

WRIGHTSVILLE BEACH, NORTH CAROLINA  
STEP-RESISTANCE GAGE  
WATER DEPTH = 17 FT

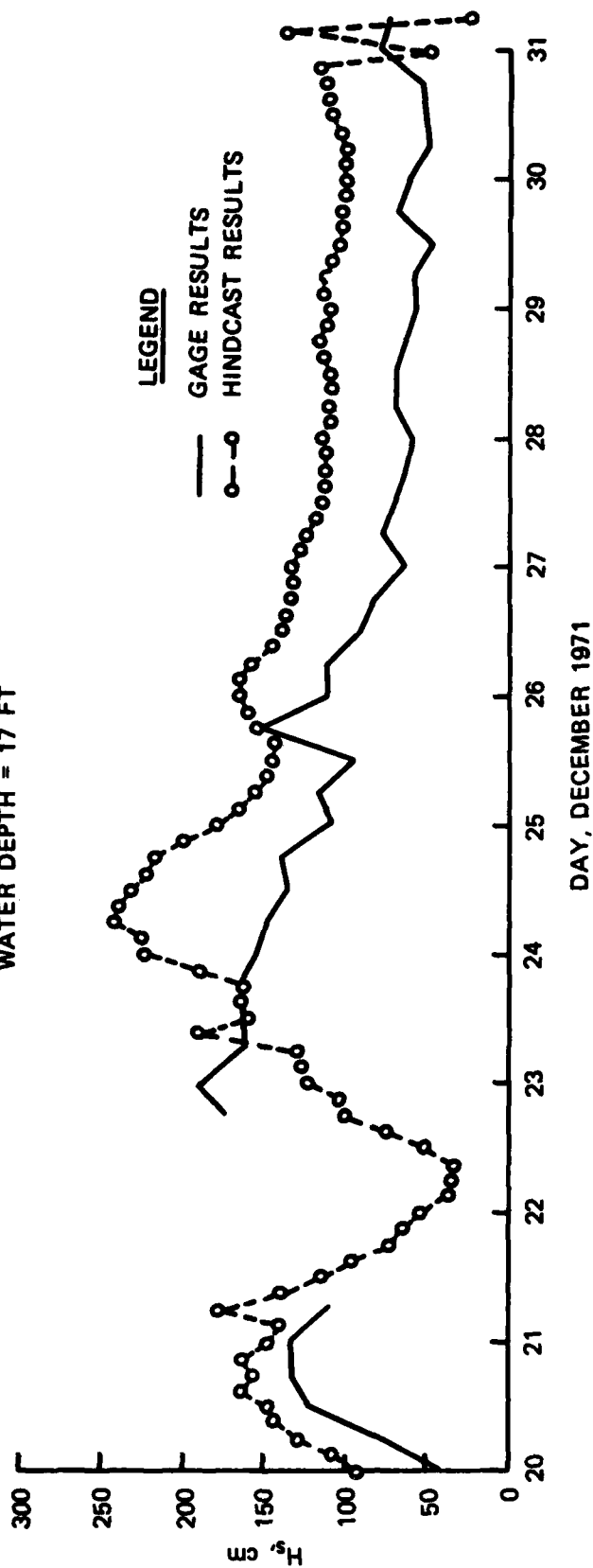


Figure C11. Plots of  $H_s$  versus time for a period in December 1971 for  
Wrightsville Beach, North Carolina

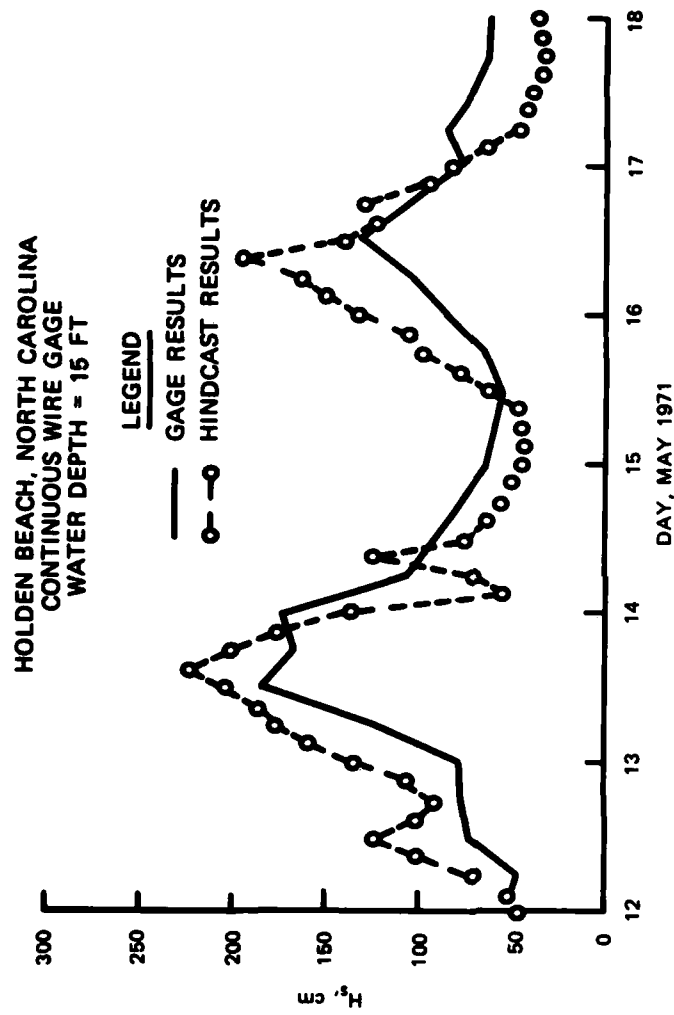


Figure C12. Plots of  $H_s$  versus time for a period in May 1971 for  
Holden Beach, North Carolina

HOLDEN BEACH, NORTH CAROLINA  
CONTINUOUS WIRE GAGE  
WATER DEPTH = 15 FT

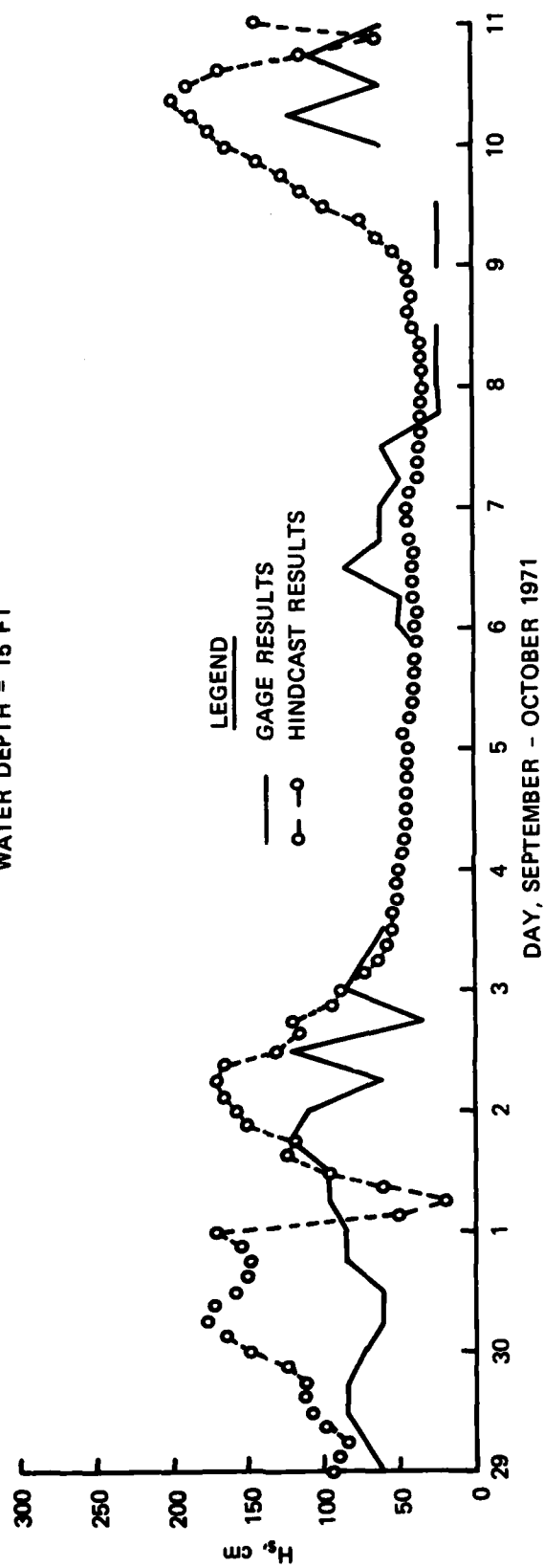


Figure C13. Plots of  $H_s$  versus time for a period in September-October 1974 for Holden Beach, North Carolina



DAYTONA BEACH, FLORIDA  
PRESSURE GAGE  
WATER DEPTH - 11 FT

LEGEND  
— GAGE DATA  
○—○ HINDCAST DATA

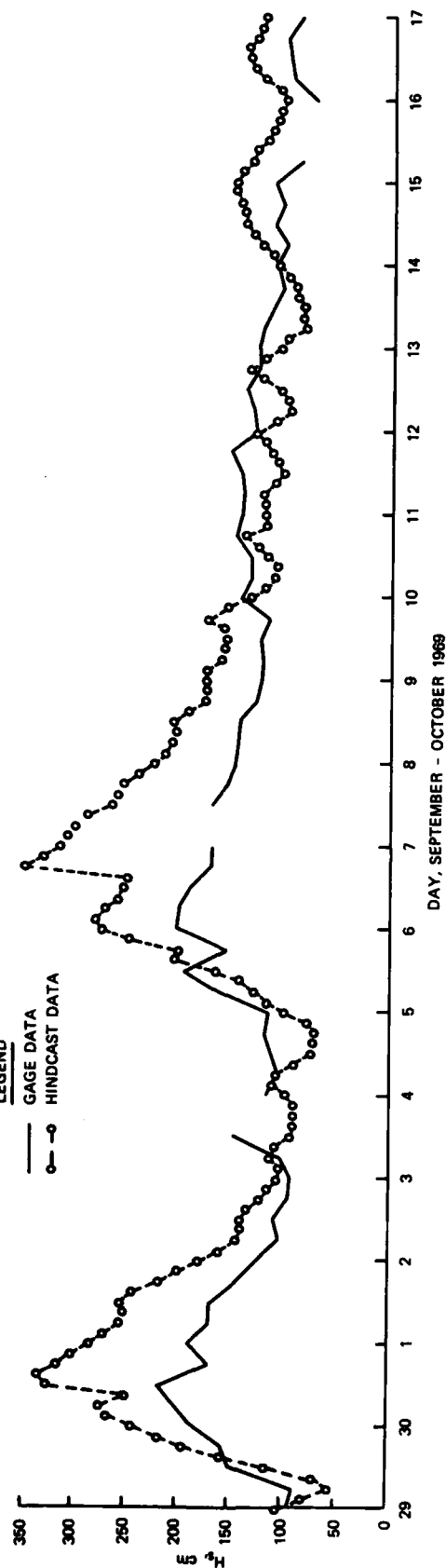


Figure C14. Plots of  $H_s$  versus time for a period in September-October 1969 for Daytona Beach, Florida

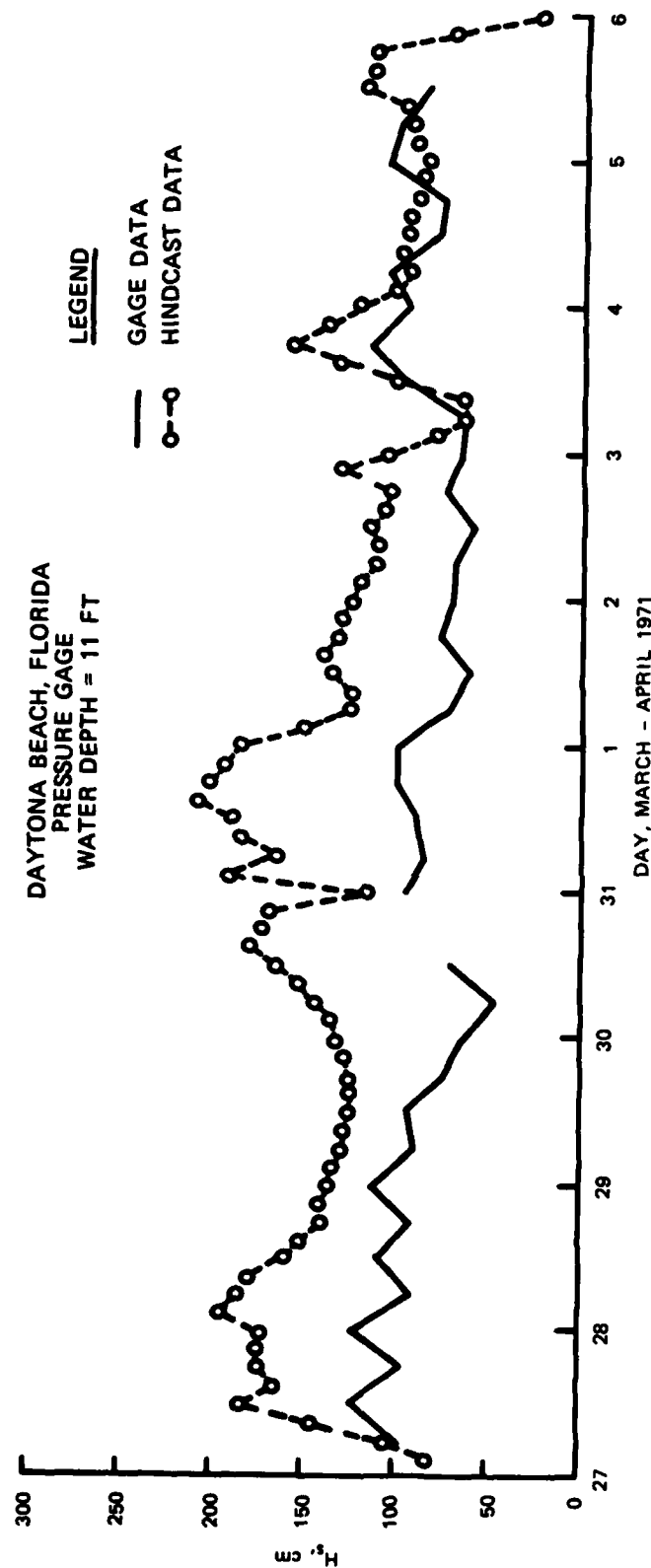


Figure C15. Plots of  $H_s$  versus time for a period in March-April 1971 for Daytona Beach, Florida

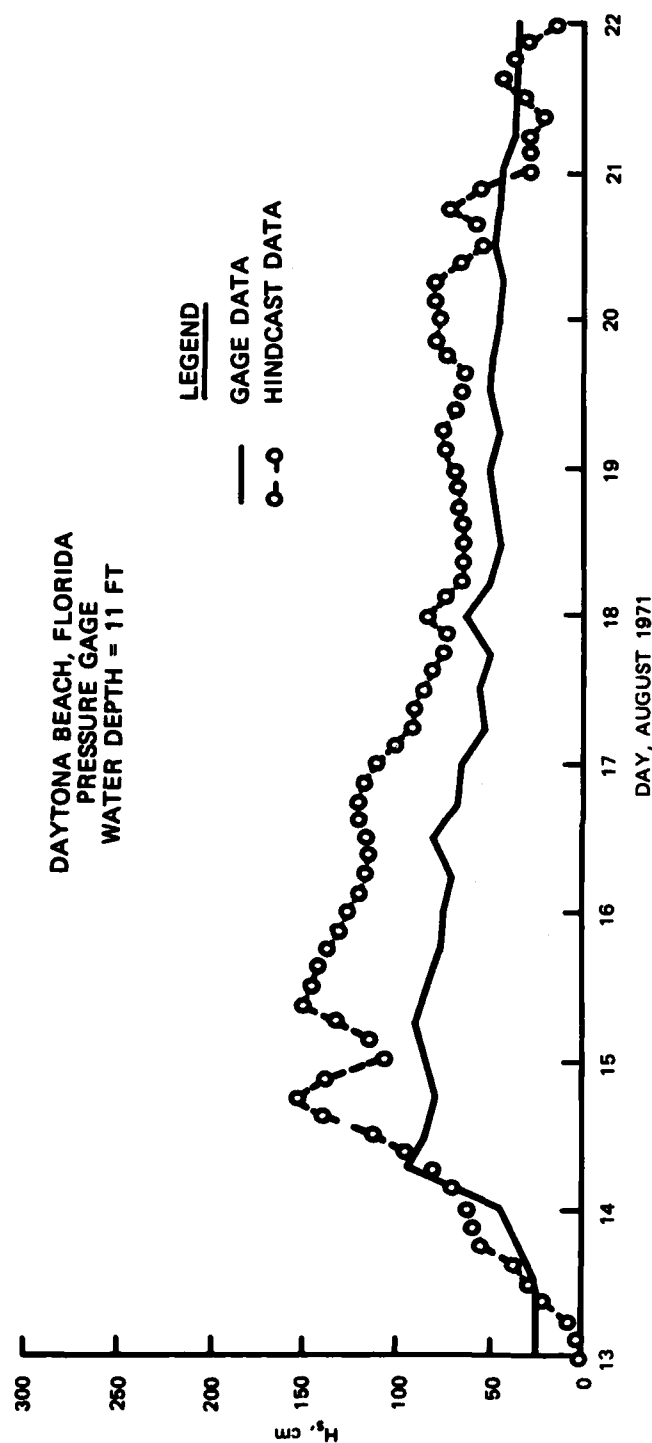


Figure C16. Plots of  $H_s$  versus time for a period in August 1971 for  
Daytona Beach, Florida

# Appendix D: Notation

Symbol	Definition
$c$	Phase velocity of the wave component
$c_g$	Group velocity of the wave component
$E_o$	Total deepwater spectral energy
$E_s$	Total shallow water spectral energy
$E_t$	Total integrated spectral wave energy
$E_L$	Total spectral energy loss due to wave-wave interactions
$E_1(f)$	One-dimensional spectrum
$E_2$	Two-dimensional spectrum
$f$	Frequency
$f_c$	Cutoff frequency
$f_m$	Frequency of the spectral peak
$F_2$	Two-dimensional wave spectrum in wave number $(k)$ space
$g$	Acceleration due to gravity
$h$	Water depth
$H$	Wave height
$i$	Frequency increment
$I_n$	Incremental values of the deepwater parameter
$j$	Angle increment
$k$	Wave number modulus
$(k)$	Wave number space
$m_i$	Number of intervals used to resolve the $i^{th}$ parameter
$M$	Momentum
$n$	Number of parameters
$n(k)$	Action density defined in terms of the wave number modulus $k$
$N$	Total number of transformations
$p(f,h)$	Matrix form of the transformation processes
$P'_i$	Nearshore wave parameter value
$R$	Nondimensional dispersion relationship
$T$	Wave period
$T_i$	Transformation matrices

Symbol	Definition
$T_p$	Peak spectral wave period
$\alpha$	Phillips equilibrium constant
$\delta$	Spectral shape function
$\Delta_j$	Coefficient flagging wave sheltering
$\varepsilon$	Dimensionless constant, dependent on the breaking limit
$\theta$	Direction
$\theta_o$	Deepwater wave angle
$\bar{\theta}$	Central angle of the spectrum
$\lambda$	Constant
$\Lambda_{ij}$	Matrix of precomputed values of $\rho(f,h)$ in discrete form
$\phi$	Normalized angular distribution function
$\phi(\omega_h)$	Nondimensional function
$\omega_m$	Radial frequency of spectral peak
Subscript	
o	Deepwater conditions

**END**

**FILMED**

**12-83**

**DTIC**